MAGNETOCRYSTALLINE ANISOTROPY, MAGNETOSTRICTION AND SATURATION MAGNETIZATION OF $SmCo_5$ SINGLE CRYSTALS
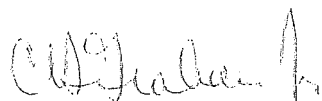
2003 - 2

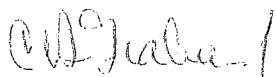Stanley Richard Trout

A DISSERTATION

in

Metallurgy and Materials Science

Presented to the Graduate Faculties of the University of Pennsylvania in Partial Fulfillment of the Requirements for the degree of Doctor of Philosophy.

1979

_____
Supervisor of Dissertation

_____
Graduate Group Chairman

ACKNOWLEDGEMENTS

TABLE OF CONTENTS

LIST OF FIGURES

v

LIST OF TABLES AND PROGRAMS

CHAPTER I.

INTRODUCTION

The history of rare earth-cobalt (hereafter referred to as RECo) permanent magnets can be traced back to 1935 when Urbain, Weiss and Trombe[1] discovered that gadolinium is ferromagnetic. At that time, it was difficult to study the magnetic properties of other Lanthanide series elements due to the unavailability of pure rare earth metals. Rare earth ores generally contain several rare earth oxides mixed together. A program sponsored by the Atomic Energy Commission developed the ion-exchange method for separating rare earths from each other in 1947.[2] Isolated rare earth elements were made available in small quantities at reasonable cost.

Nassau, Cherry and Wallace[3], in 1960, used x-ray diffraction to determine the crystal structures of the RCo_5 compounds where R represents yttrium or a rare earth. They found all RCo_5 compounds have the $CaCu_5$ crystal structure, which is shown in Fig. 1 for $SmCo_5$. Also, in 1960, Hubbard, Adams and Gilfrich[4] reported the permanent magnet properties of $GdCo_5$. (Permanent magnet properties are defined in Fig. 2.) They found that the c-axis is the easy magnetic axis and single crystal particle alignment by an externally applied field was used to increase the remanent magnetization. They concluded that the huge coercivity (H_{ci}=8kOe) is due to the large magnetocrystalline aniostropy of $GdCo_5$. Initially their work was ignored due to the high cost of gadolinium, the low energy product of $GdCo_5$ permanent magnets and the

1

$$Sm\,Co_5$$

$\bigcirc$ – Sm

O – Co
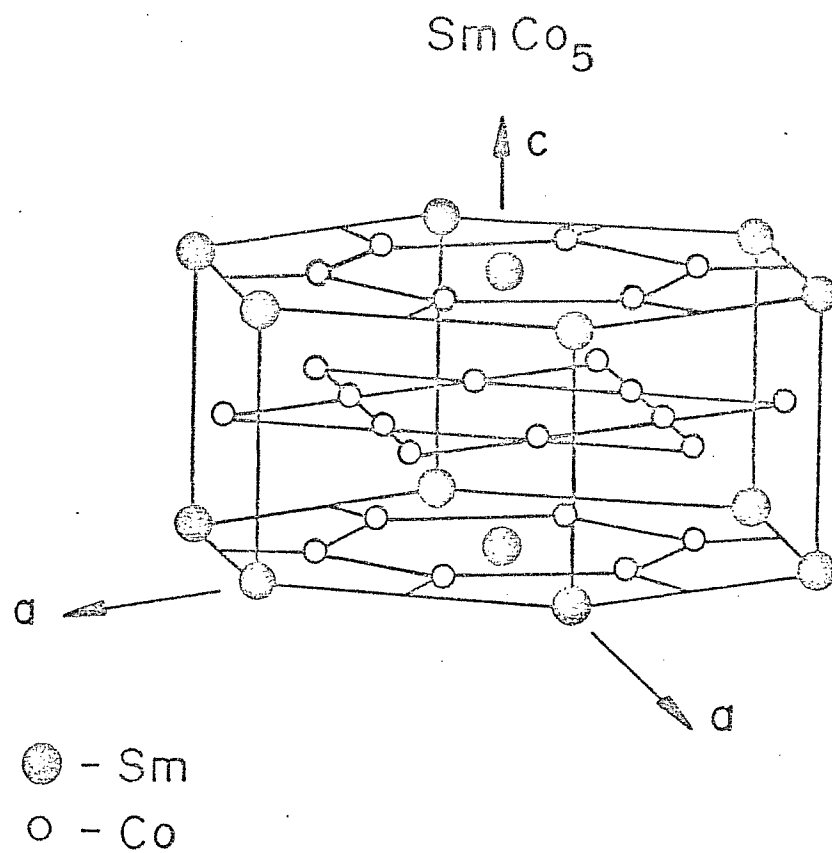
Fig. 1. Crystal structure of SmCo$_5$.
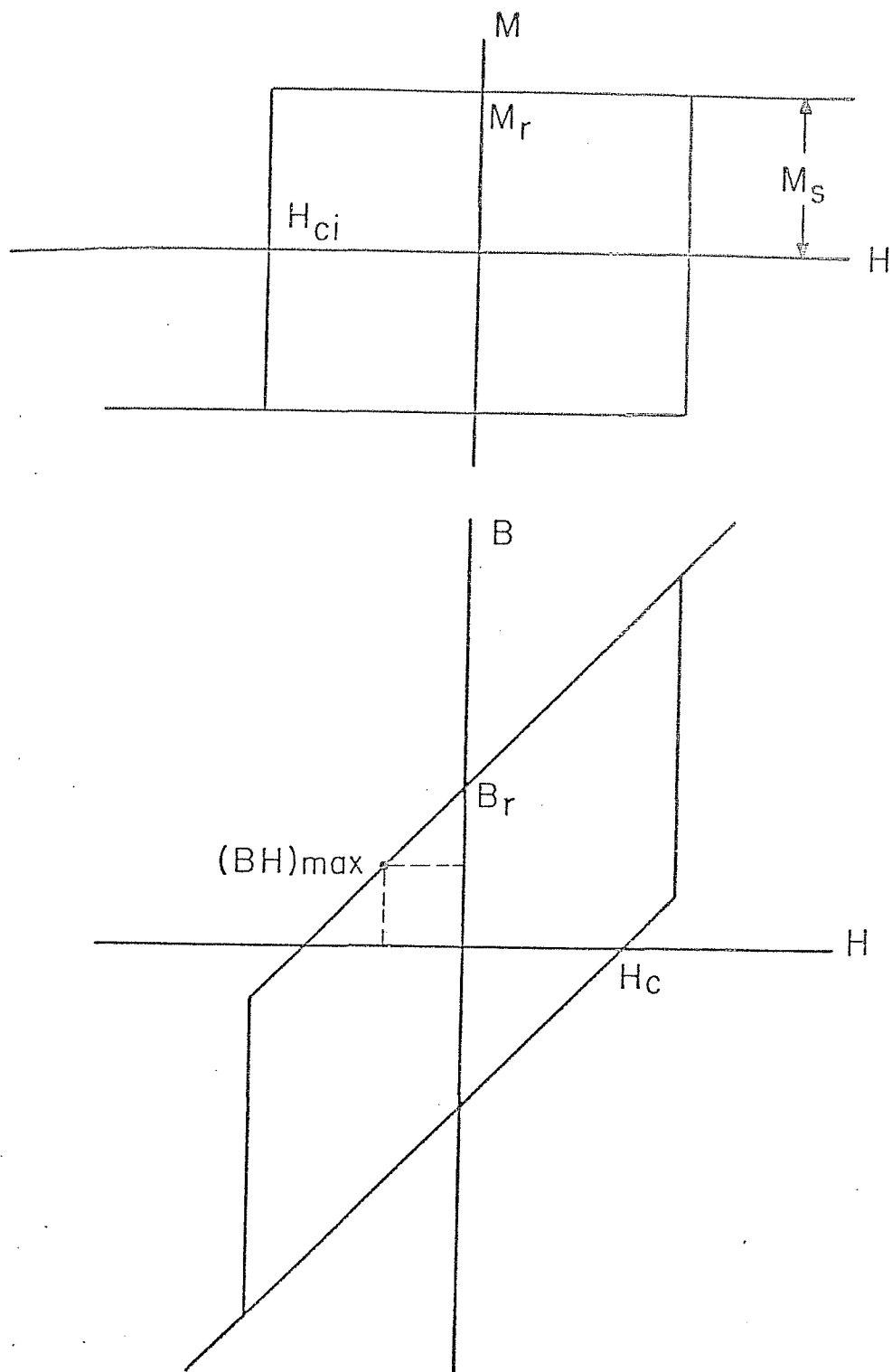
Fig. 2. Definitions of some important permanent magnet parameters. Shown here are the M vs. H and B vs. H curves for an ideal high coercivity permanent magnet material in Gaussian units, $B = H + 4\pi M$. Note that for the ideal case, $M_s = M_r$ and $(BH)_{max} = (4\pi M_s)^2/4$. Often the measured $(BH)_{max}$ is lower than the ideal maximum, so generally $(BH)_{max} \leq (4\pi M_s)^2/4$.

failure to recognize that $GdCo_5$ is part of a family of RECo compounds with similar magnetic properties.

Hoffer and Strnat[5] reported the large magnetocrystalline anisotropy of YCo_5 in 1966. Their work prompted examination of the magnetic properties of all the RCo_5 compounds. A summary of the physical and magnetic properties of these compounds is given in Table I, and the B vs. H demagnetizing curves of RECo and conventional permanent magnets are shown in Fig. 3. There are several excellent reviews of the development of RECo permanent magnets.[6,7,8,9]

Of all the RCo_5 compounds, permanent magnets based on $SmCo_5$ have the best properties for two major reasons:

1. $SmCo_5$ has the highest Curie temperature, T_c=984 K.[10]

2. $SmCo_5$ has the highest anisotropy, K_1=2.4x10^8 erg/cm^3 at

   room temperature, and K_1 is not very dependent on composition.

However, the intrinsic properties of the RCo_5 compounds cannot explain why $SmCo_5$ permanent magnets have the largest coercive fields, H_{ci}>20 kOe.

In practice, commercial $SmCo_5$ magnets are produced by liquid phase sintering.[11] In the most common method, two alloys, one nearly $SmCo_5$ and the other samarium-rich $SmCo_5$ ($\sim$36 atomic % Sm), are prepared by induction melting. The two alloys are ground into powders with an average particle diameter of 4 microns. Generally, each particle is a single crystal. The two powders are loosely mixed to a density of about 3.4 g/cm^3 and a magnetic field of 20 kOe or greater is applied to the mixed powder to align the c-axis of each particle with the field. The powder is pressed slightly to prevent particles

TABLE I

MAGNETIC AND PHYSICAL PROPERTIES OF SOME RCo_5 PHASES

Phase	T_c (K)	M_s (emu/cm^3)	ideal (BH)$_{max}$ (MGOe)	H_A (kOe)	K_1 (10^7 erg/cm^3)	Density (g/cm^3)	T_l (K)	T_p (K)
YCo_5	921	844	28.1	130	5.5	7.69	1635	1625
$LaCo_5$	840	723	20.6	175	6.3	8.03	1490	1363
$CeCo_5$	647	612	14.8	170-210	5.2-6.4	8.55	1480	1469
$PrCo_5$	885	955	36.0	145-210	6.9-10.0	8.34	1520	1505
$SmCo_5$	997	768	23.0	210-290	8.1-11.2	8.60	1600	1593
$(MM)Co_5$	795	708	19.8	180-195	6.4-6.9	8.35	–	1458

(MM) = mischmetal; properties quoted are for a commercial mischmetal containing, in atomic percent, 54.4% Ce, 26% La, 13% Nd and 5% Pr.

T_c = Curie temperature

T_l = liquidus temperature

T_p = temperature of peritectic reaction

The ideal (BH)$_{max}$ is calculated from $(4\pi M_s)^2/4$ and is not an experimental value.

(reference 31)
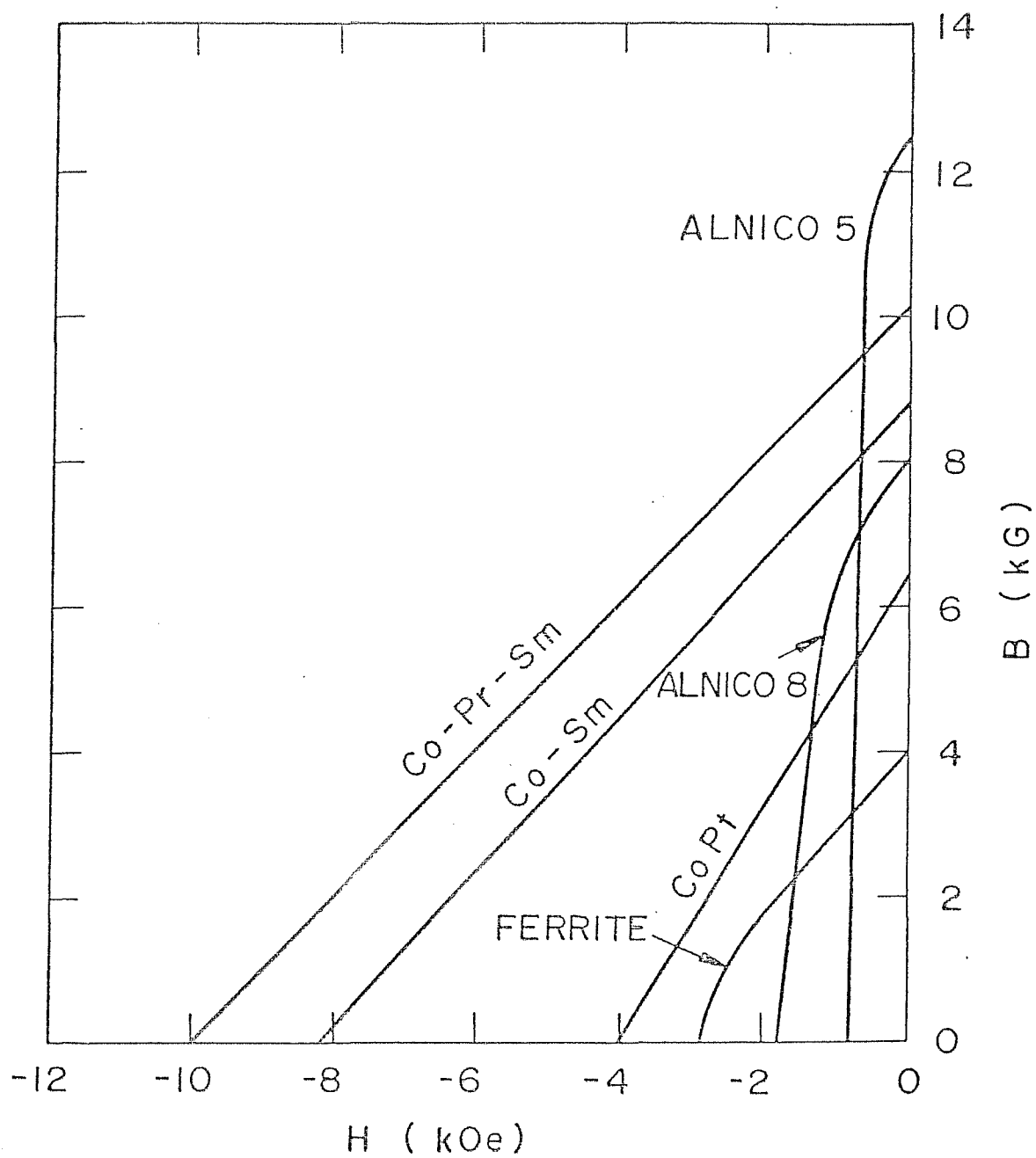
Fig. 3. Second quadrant B vs. H curves for common permanent magnet
         materials.

from rotating out of alignment when the field is removed. Then the powder is pressed to roughly 1×10^9 N/m^2 and sintered at 1100°C for about 30 minutes. The composition of the samarium-rich alloy, sometimes called the sintering aid, is chosen so that it has a liquid phase component at the sintering temperature which helps to increase the final density of the material. Post-sintering heat treatments are used to increase the coercivity. Commercial SmCo$_5$ magnets are produced with nearly the ideal $(BH)_{max}$ and are used in travelling wave tubes, watt-hour meters, electric motors, wrist watches, magnetic bearings and other applications where size and weight are important considerations.

At present, the immediate future of RECo magnets is uncertain. Most of the free-world cobalt comes from Zaire as a by-product of copper mining. However, the cobalt supply was curtailed for six months in 1978 due to the political unrest in that part of Africa. The decrease in the cobalt supply has caused the price of cobalt to triple over the past year. While current supplies are returning to the previous levels, the present forecast is that the price of cobalt will fall, but not to previous levels.

The cobalt shortage has had an unsettling effect on the permanent magnet industry. Since the design of a magnetic circuit requires a substantial capital investment, users of permanent magnets have been reluctant to redesign a product to use SmCo$_5$ magnets. Consequently, Alnico magnets are used in many products where SmCo$_5$ magnets would cost less. However, since cobalt is a major component of Alnico

magnets, there is pressure on users to change to either oxide magnets, barium or strontium ferrite, which are cobalt-free or to RECo magnets which use cobalt more efficiently than Alnico magnets.

The long range future for RECo permanent magnets is encouraging. In time, $SmCo_5$ and other RECo permanent magnets will replace Alnico or ferrite magnets in many applications and become a significant proportion of the permanent magnet industry. In these applications, RECo magnets will be used because they do the job more effectively than their competitors, considering size, weight or cost. There is also an interesting future for RECo magnets in new applications where they are uniquely suited because of their high energy product or large coercivity. There have already been some successful human implant applications of $SmCo_5$ magnets.

Future developments in RECo magnets will probably concentrate in three areas. First, it is desirable to increase the saturation magnetization since it limits the energy product, $(BH)_{max} \leq (4\pi M_s)^2/4$. To achieve this goal, there are several possibilities such as R_2Co_7 and R_2Co_{17} compounds, or additions of iron to an RECo compound.[12,13,14] Unfortunately, work in this area has produced permanent magnets with substantially lower coercive fields than $SmCo_5$ magnets. Future research may improve the coercive fields in these compounds. Second, it is desirable to decrease the cost of RECo magnets to make them more competitive with other permanent magnet materials. Work in this area has concentrated in substituting less expensive mischmetal for samarium.[15,16,17] Since removing the samarium lowers M_s, $(BH)_{max}$ and

H_{ci}, there have been several studies to determine the trade-offs between cost and magnetic properties. This work is also important if there is a sudden increase in the demand for samarium because of the present limitations on refining facilities. New research may be in the area of finding other substitutions of this type for either samarium or cobalt since cobalt is now more expensive than samarium. In fact, a scientist from the General Motors Research Laboratories has remarked that their goal is to make samarium-cobalt permanent magnets with neither samarium nor cobalt. The cost of RECo magnets could also be lowered by improved production methods. There has been some successful work with casting RECo permanent magnets.[18] Third, there will be further work in improving certain properties for specific purposes. For example, there has been research into the area of reducing the temperature dependence of the saturation magnetization around room temperature for RECo magnets to be used in microwave applications.[19]

Even though $SmCo_5$ is an extensively used permanent magnet, data on the intrinsic properties of the material is incomplete. In part, the deficiency is due to its large magnetocrystalline anisotropy. Consequently, the anisotropy constants and magnetostriction constants are difficult to measure with the limited magnetic fields available in most laboratories. Therefore, high field magnet facilities such as the High Field Magnet Laboratory at the University of Pennsylvania are required to measure some intrinsic properties of $SmCo_5$.

A complete knowledge of the temperature dependence of the intrinsic

properties (magnetocrystalline anisotropy, magnetostriction and saturation magnetization), is necessary since they ultimately determine the potential of a material as a permanent magnet. In this work, the saturation magnetization, magnetocrystalline anisotropy and magnetostriction of $SmCo_5$ single crystals have been measured as a function of temperature from 4.2 K to room temperature and above. This experiment overcomes the three major problems that beset earlier experiments: low magnetic fields, powder samples and off-stoichiometric compositions, by using a set of high quality single crystal samples cut from the same ingot, and by using large magnetic fields.

CHAPTER II

SAMPLES

A bulk $SmCo_5$ single crystal was prepared by the Bridgman method by A. E. Austin and J. F. Miller at the Battelle Columbus Laboratory for the Air Force Materials Laboratory, Wright-Patterson Air Force Base, Ohio.[20] The lattice parameters measured by Austin and Miller were a=4.999 Å and c=3.972 Å with an error of $\pm$ 0.002 Å measured by Debye-Scherrer x-ray diffraction patterns. This single crystal was made available to D. A. Doane of this laboratory by H. J. Garrett of the Air Force Materials Laboratory.

Before the samples were cut from the single crystal, Doane[6] did an extensive Laue x-ray study of the crystal to verify single crystallinity and to orient the crystal for subsequent spark cutting. Discs 9.0 mm in diameter and 1.5 mm thick were spark cut from the bulk single crystal for the orientations needed to measure magneto-striction and elastic constants. This size was determined to be thin enough so the form effect could be ignored and thick enough so the unbonded surface of the sample could deform freely.[6] Some surface cracks were observed by Doane at the time the crystals were cut. Later, the cracks caused chipping in the Doane experiments and catas-trophic shattering and twisting of some samples in this study. After spark cutting, Doane mechanically polished and electropolished the samples to remove any residual surface stress. Laue photographs were used to verify that the sample surfaces were indeed stress-free.

11

The density of a large piece of scrap single crystal was measured by finding its mass in air and in water. The measured density of $SmCo_5$ at $23^{\circ}C$ was 8.559 g/cm^3. This result agrees within 0.5 % of the three published values. Buschow and Velge[21] give 8.53 g/cm^3, Haszko[22] gives 8.58 g/cm^3 and Searle et al.[23] give the density as 8.60 g/cm^3. The measured density also agrees with the density calculated from the lattice parameters given for this single crystal, 8.596 g/cm^3.

CHAPTER III

SATURATION MAGNETIZATION

Theory

In a ferromagnetic substance, the maximum magnetic moment of the bulk material is the saturation magnetization. This corresponds to the complete alignment of all the atomic magnetic moments along the direction of measurement. There are two measures of the saturation magnetization in a sample, the moment/mass, σ_S, (emu/g in CGS units) and the moment/volume, M_S, (emu/cm^3 in CGS units). The moment/mass and the moment/volume are related to the density by

(1) M_S / σ_S = density.

The moment/volume, M_S has greater practical importance and is used in fundamental theory such as Maxwell's equations. However, when the saturation magnetization is measured as a function of temperature, σ_S is generally used since the volume of the sample is a function of temperature while the mass is not.

In SmCo$_5$, the magnitude of the saturation magnetization is due almost entirely to the magnetic moment of the cobalt atoms. A simple estimate of the saturation magnetization at $T = 0$ K can be made by assuming that only cobalt atoms contribute to the magnetization and that the moment of a cobalt atom is the same in SmCo$_5$ as it is in pure cobalt

(2) $\sigma_0 =$

$$\frac{(5 \text{ Co atoms/unit cell})(1.715 \ \mu_B/\text{Co atom})(0.927 \times 10^{-20} \ \text{emu}/\mu_B)}{(7.389 \times 10^{-22} \ \text{g/unit cell})}$$

$= 107.6$ emu/g

13

or $M_0 = 932$ emu/cm^3. Streever,[49] using NMR, finds an Sm moment of 0.39 μ_B and estimates the Co moment as 1.63 μ_B to make the total moment consistent with saturation magnetization measurements at 0 K, $\sigma_0 = 107.1$ emu/g. However, this estimate for the Sm moment may be too large since Klein and Menth find almost no difference between the saturation magnetization of SmCo$_5$ and YCo$_5$, where the Y^{+3} ion has no magnetic moment.[29]

The temperature dependence of the saturation magnetization is due to the thermal vibrations of the spin moments. The contribution of each moment to the net magnetization is lowered by the vibrations. As the temperature increases, the moments deviate further from the saturation direction and the saturation magnetization decreases to zero at the Curie temperature. At that point, the thermal energy is roughly twice the exchange energy.

Information about the temperature dependence of the saturation magnetization is important from a theoretical point of view. The Callen and Callen single-ion theory predicts the temperature dependence of the magnetocrystalline anisotropy and the magnetostriction based on the temperature dependence of M_s.[24]

For a permanent magnet material, the saturation magnetization and its temperature dependence are important considerations. First, M_s is the upper limit of the remanent magnetization, M_r. Commercial SmCo$_5$ magnets have a remanence that is at least 90% of the saturation magnetization. Second, in a high coercivity material such as SmCo$_5$, $(H_c \sim 4\pi M_s)$, the maximum energy that can be stored in the material $(BH)_{max}$, is limited by $(4\pi M_s)^2/4$. Therefore, it is desirable to have a large M_s and to have it change as little as possible over the working temperature

range of the magnet since a 5% decrease in M_s can cause a 10% decrease in $(BH)_{max}$. In practice these criteria are simplified to call for a high Curie temperature and a large saturation magnetization.

Experiment

The saturation magnetization was measured using a vibrating sample magnetometer (VSM) and a conventional iron-core electromagnet. The complete experimental apparatus is shown in Fig. 4. An iron sample was used as a calibration standard at room temperature and at 77 K. A single crystal of $SmCo_5$ was mounted in the VSM with its easy axis parallel to the field. The electromagnet produced a maximum field of about 8 kOe which was sufficient to saturate the sample. The magnetization was detected by four pick-up coils mounted on the magnet pole pieces. Their signal was amplified and converted by the lock-in amplifier into a d.c. signal proportional to the magnetization. The output signal was recorded as the Y axis on the X-Y recorder.

A copper-constantan thermocouple was attached directly to the sample by copper paint. The thermocouple voltage was fed to the X axis of the X-Y recorder.

The sample was enclosed by a small glass dewar. After the saturation magnetization was measured at 77 K, the liquid nitrogen was allowed to boil off. The saturation magnetization was recorded as the sample warmed up. The sample could warm up from 77 K to 220 K in about 30 minutes. This time was fast enough to avoid output drift in the lock-in amplifier and slow enough to assure that the thermocouple and the sample were at substantially the same temperature. Above room temperature, the
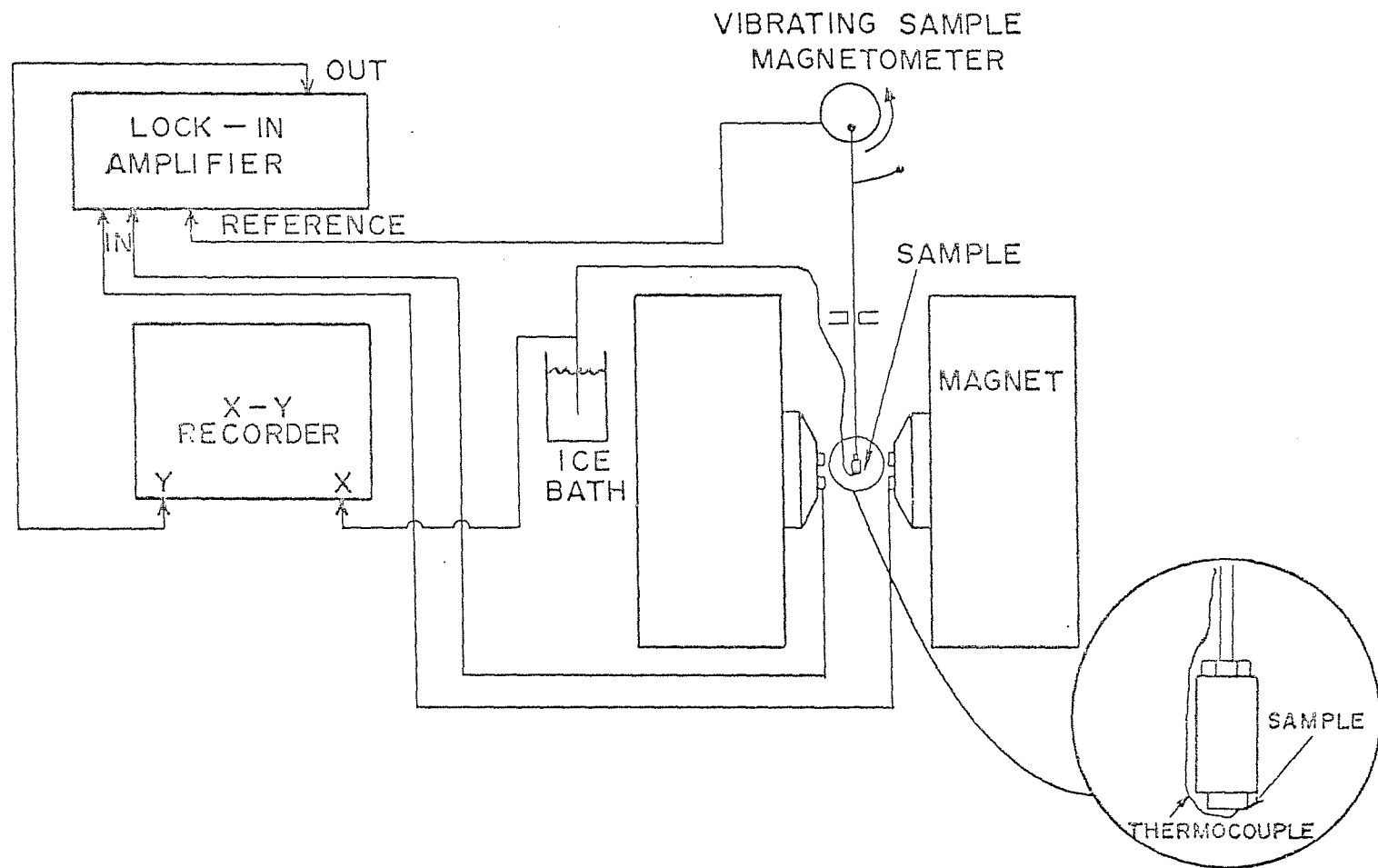
Fig. 4. Vibrating sample magnetometer used to measure saturation magnetization as a function of temperature.

sample was enclosed in a heater and warmed from 300 K to nearly 900 K, again in about 30 minutes. The sample was protected from oxidation by a high temperature alumina cement. On cooling, the curve was reversible.

Results

The saturation magnetization results are shown in Table II and plotted in Figs. 5 and 6.

The σ_S vs. T results were obtained directly from the experimental curves, while the M_S vs. T data were derived from the σ_S vs. T data using the density of $SmCo_5$ at the temperature in question and eq. (1). The density of $SmCo_5$ measured at $23^{\circ}C$ was 8.559 g/cm^3. There are no data on the temperature dependence of the density of $SmCo_5$. However, this information can be derived from the x-ray data of Martin, Benz and Rockwood[25] on the variation of the unit cell volume in sintered $SmCo_5$ magnets. Their data show the variation to be linear over the range of measurement, 77 to 300 K, and that the temperature dependence is not sensitive to small changes in composition around $SmCo_5$. Therefore, these data are used to calculate M_S from σ_S, using the fact that the volume of the unit cell is inversely proportional to the density. This means,

$$(3) \quad \rho(T) = \rho(T=296K) \frac{V(T=296K)}{V(T)}$$

so that

$$(4) \quad M_S(T) = \sigma_S(T) \rho(T=296K) \frac{V(T=296K)}{V(T)} .$$

From the Martin, Benz and Rockwood data,

TABLE II

SATURATION MAGNETIZATION DATA

T (K)	T ($^\circ$C)	T/T_c	σ_s (emu/g)	σ/σ_0	M_s (emu/cm^3)	M/M_0	$(M/M_0)^3$	$4\pi M_s$ (kG)	M_{est} (emu/cm^3)
0	-273	0	108	1	932	1	1	11.71	932
77	-196	.078	106.7	.988	919	.986	.960	11.55	919
87	-186	.088	106.3	.984	916	.982	.948	11.51	916
113	-160	.115	105.5	.977	908	.974	.924	11.41	909
136	-137	.138	104.8	.970	901	.967	.904	11.32	901
156	-117	.159	103.9	.962	893	.958	.879	11.22	894
174	-99	.177	103.4	.957	888	.953	.865	11.16	887
191	-82	.194	102.6	.950	881	.946	.846	11.08	881
208	-65	.221	101.6	.941	872	.936	.820	10.96	874
220	-53	.224	101.2	.937	868	.932	.809	10.91	869
295	+22	.300	98.8	.915	846	.907	.747	10.63	833
345	72	.351	96.5	.894	825	.885	.694	10.37	807
388	115	.394	95.9	.888	819	.879	.679	10.29	783
429	156	.436	94.9	.879	809	.868	.655	10.17	759
486	213	.494	92.3	.854	785	.843	.599	9.87	724

TABLE II
(continued)
SATURATION MAGNETIZATION DATA

T (K)	T (^{o}C)	T/T_c	σ_s (emu/g)	σ/σ_0	M_s (emu/cm^3)	M/M_0	$(M/M_0)^3$	$4\pi M_s$ (kG)	M_{est} (emu/cm^3)
516	243	.524	91.0	.843	774	.831	.574	9.73	704
569	296	.578	88.6	.820	752	.807	.526	9.46	668
592	319	.602	86.8	.803	736	.790	.493	9.25	652
619	346	.629	85.5	.792	725	.778	.472	9.12	633
672	399	.683	81.5	.754	690	.740	.406	8.67	593
728	455	.740	76.4	.707	646	.693	.333	8.11	550
768	495	.780	70.8	.655	598	.641	.264	7.51	518
793	520	.806	67.7	.627	571	.613	.231	7.18	498
813	540	.826	65.3	.604	551	.591	.206	6.92	481
823	550	.836	62.6	.580	528	.567	.182	6.64	473
838	565	.852	59.8	.553	504	.541	.158	6.33	460
843	570	.857	57.7	.535	487	.522	.142	6.11	456
848	570	.862	55.5	.514	468	.502	.126	5.88	452
868	595	.882	51.4	.472	433	.465	.100	5.44	435
883	610	.897	49.0	.454	412	.442	.087	5.18	422

TABLE II
(continued)
SATURATION MAGNETIZATION DATA

$T_c = 984$ K from reference 10.

M_{est} is calculated using eq. (4) and eq. (8) with $B = 0.644$.

The saturation magnetization at $T = 0$ K was calculated using eq. (8).
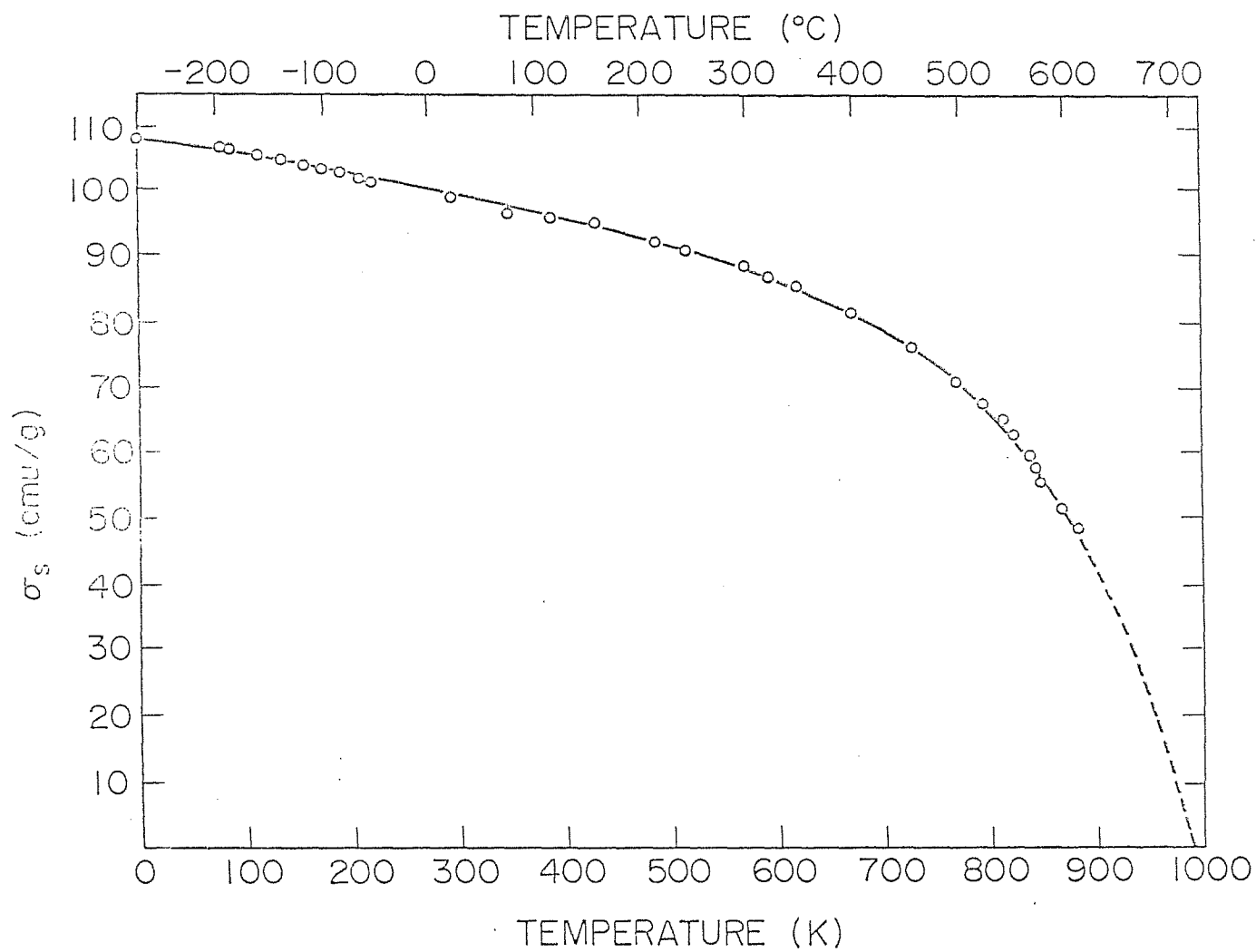
Fig. 5. Saturation magnetization plotted against temperature, σ_s vs. T.
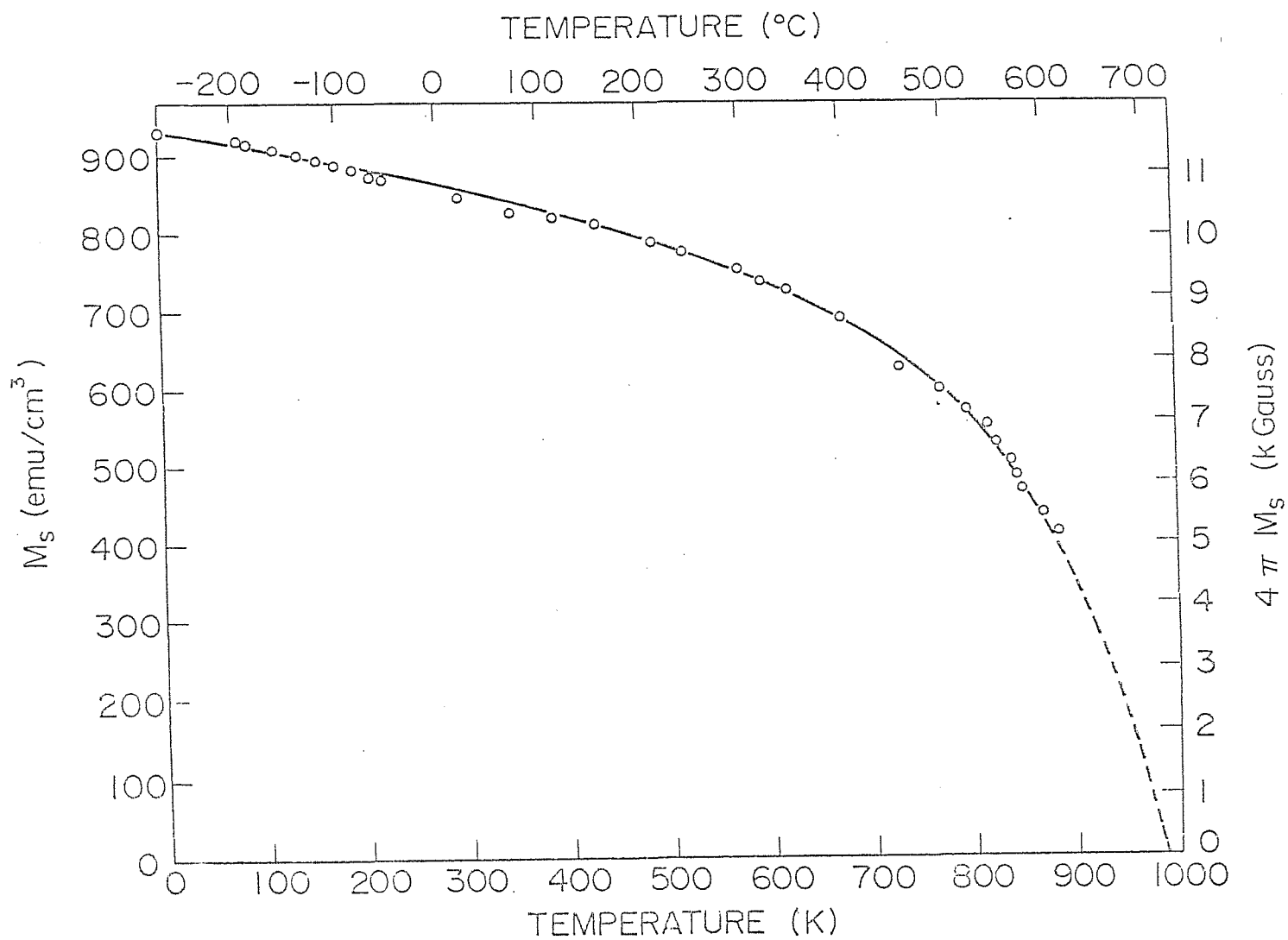
Fig. 6. Saturation magnetization plotted against temperature, M_s vs. T.

(5) $V(T)$ (Å^3) $= 85.33 + 0.002491\ T$ (K)

over the range 77 to 300 K. The M_s data given in Table II is calcu-

lated using eq. (4) and assuming that eq. (5) is reasonably accurate

over the entire temperature range of the experiment.

Comparison of the Results to Theory

The temperature dependence of the saturation magnetization can

be examined theoretically by considering either the molecular field

or spin-waves.

Briefly, the molecular field, proposed by Weiss in 1907,[26] is

the field experienced by a single atomic spin due to its neighbors.

If one assumes the classical view that the spins can have any orienta-

tion, the temperature dependence of the saturation magnetization is

given by the Langevin function,

(6) $\sigma/\sigma_0 = L(a) = \coth(a) - 1/a$

where $a = (\sigma/\sigma_0)(3T_c/T)$, $\sigma = \sigma_s(T)$ and $\sigma_0 = \sigma_s(T = 0\ K)$. The classical

$J = \infty$ curve is generated by this equation and is plotted in Fig. 7.

Quantum theory modifies the classical argument by requiring that

the angular momentum be quantized. The relative magnetization is given

by the Brillouin function,

(7) $\sigma/\sigma_0 = \left[\dfrac{2J + 1}{2J}\right] \coth\left[\dfrac{2J + 1}{2J}\ a'\right] - \left(\dfrac{1}{2J}\right) \coth\left(\dfrac{a'}{2J}\right)$

where $a' = (\sigma/\sigma_0)(3J/J + 1)(T_c/T)$. Note that as J becomes large,

eq. (7) approaches the classical case, eq. (6). If the magnetic mo-

ment is due entirely to spin, $J = \frac{1}{2}$. The relative saturation magneti-

zation curves for $J = \frac{1}{2}$ and $J = 1$ are shown in Fig. 7.

The experimental results of relative saturation vs. relative
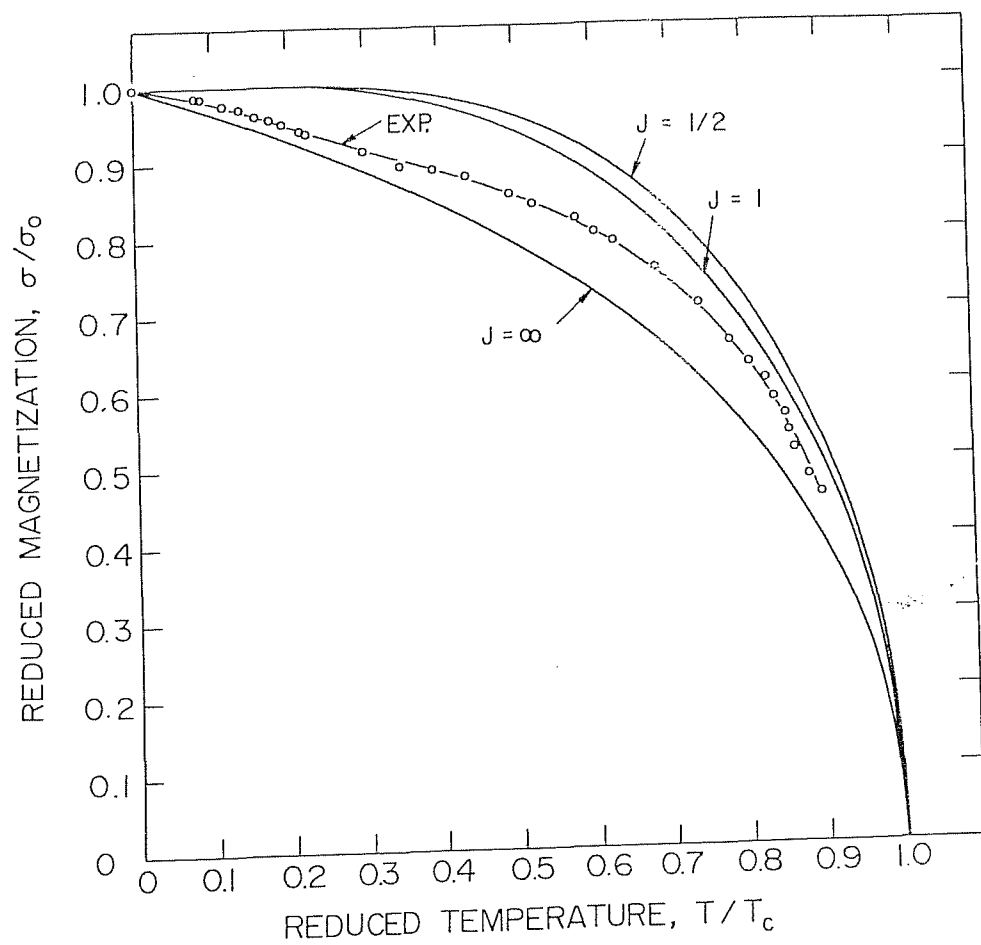
Fig. 7. Theoretical temperature dependence of the saturation
magnetization compared to experimental results.

temperature are also shown in Fig. 7. The Curie temperature for $SmCo_5$ was taken as 984 K from reference 10. Other measurements of the Curie temperature are within 20 K of this value and the data from this work indicates that the Curie temperature is in this range.

Fig. 7 shows that the experimental points are all greater than the $J = \infty$ curve and are less than the $J = \frac{1}{2}$ and $J = 1$ curves. Data for iron, nickel and cobalt show much better agreement with the $J = \frac{1}{2}$ and $J = 1$ curves than do these results for $SmCo_5$. This behavior indicates that samarium may have a small moment in $SmCo_5$ which drops off much faster than the cobalt moment with increasing temperature.

The theory of spin-waves, proposed by Bloch in 1930,[27] considers the collective precession of spins. At low temperatures, Bloch found that the temperature dependence of the saturation magnetization is given by

$$(8) \quad \sigma(T)/\sigma(T = 0) = 1 - B(T/T_c)^{3/2}$$

where B is a constant of the material. Since the saturation magnetization was not measured at $T = 0$ K, the values $M_s = 932$ emu/cm^3 and $B = 0.644$ were estimated using eq. (8), eq. (4) and the data from 77 to 220 K. This behavior was also observed in $SmCo_5$ by Kütterer et al.[48] but with $B = 0.4$.

In a highly anisotropic material, the frequency of the spin-wave is modified. Considered by Niira,[50] the temperature dependence of the saturation magnetization of Dy was explained using the concept of the spin-wave gap. Niira modified eq. (8) to predict that the saturation magnetization should vary as $B\, e^{-\Delta/kT}\, T^{3/2}$ where Δ is the spin-wave
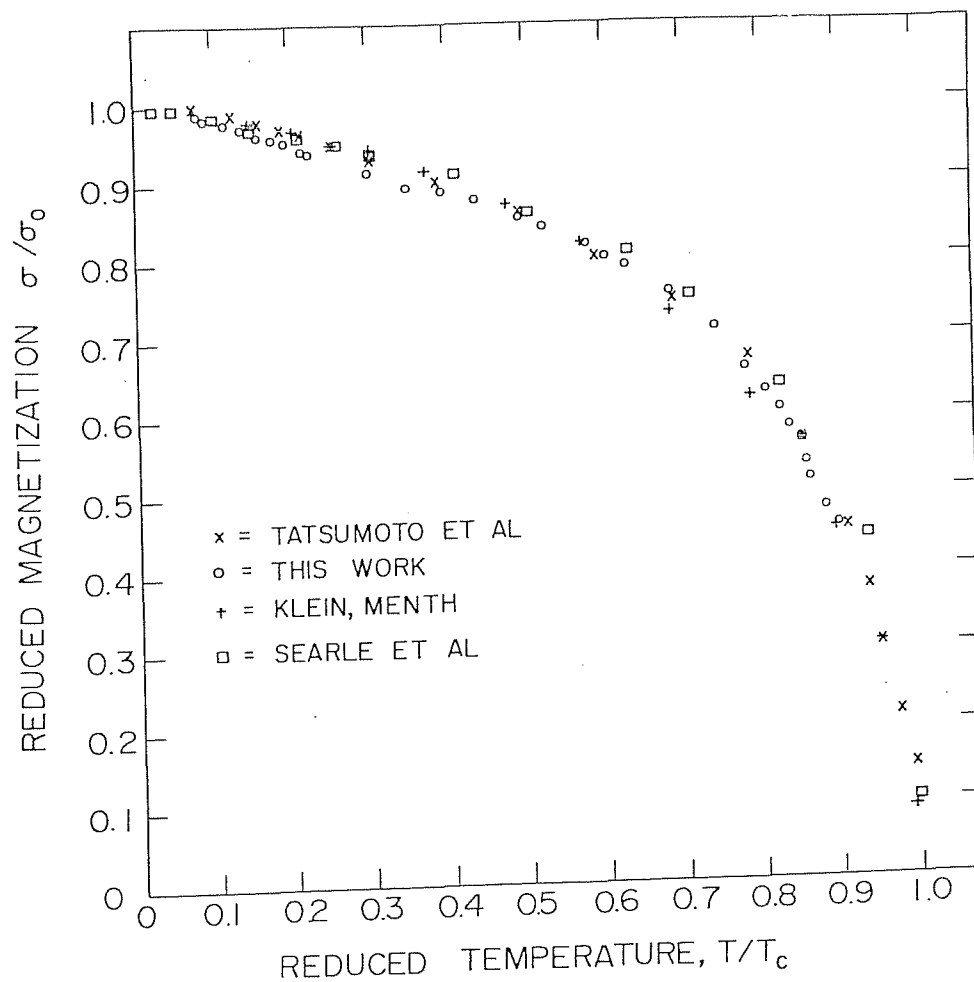
Fig. 8. Temperature dependence of the saturation magnetization compared to other experiments.

gap, $\Delta = 2k_2(T = 0)/\text{spin}$. For $SmCo_5$, $\Delta \sim 50$ K, so that the temperature dependence of the saturation magnetization may not follow $T^{3/2}$ below 77 K.

Discussion and Comparison to Earlier Experiments

The results of four other saturation magnetization vs. temperature studies and this work are plotted in Fig. 8 as reduced magnetization vs. reduced temperature. All the results show good agreement. The only area where there is some disagreement is around $T/T_c = 0.3$, near room temperature. Here the data from this work are slightly lower than the other experiments. Since the disagreement is less than 3%, it is felt that the difference is not significant.

The absolute values of the saturation magnetization experiments are summarized in Table III. This work agrees best with the Klein and Menth[29] and Ermolenko[30] results. Also, the estimated value at T = 0 K, 108 emu/g, agrees very well with the calculated estimate 107.6 emu/g. The Tatsumoto et al.[10] and Buschow and Velge[21] values are about 10% lower and the Searle et al.[23] values is 6% higher than this work. Buschow and Velge used a 100 μm powder, aligned at 40 kOe, for their measurement while the others used single crystal spheres, 1-20 mm in diameter. Tatsumoto et al. used a magnetic balance to measure the moment while the others used vibrating sample magnetometers. The applied fields ranged from 16 to 25 kOe. The disagreement with Tatsumoto et al. and Buschow and Velge may be due to variations in composition, alignment problems or an inaccurate magnetic balance.

TABLE III

SATURATION MAGNETIZATION OF $SmCo_5$

STUDY	σ_s or M_s		TEMPERATURE
Buschow and Velge[21]	90	emu/g	300 K
Tatsumoto et al.[10]	96.0	emu/g	0 K
Searle et al.[23]	971	emu/cm^3	4.2 K
	894	emu/cm^3	300 K
Klein and Menth[29]	937	emu/cm^3	0 K
Ermolenko[30]	109	emu/g	0 K
	102	emu/g	300 K
Calculated Estimate	107.6	emu/g	0 K
	932	emu/cm^3	
This Work	108	emu/g	0 K
	932	emu/cm^3	
	98.8	emu/g	295 K
	845	emu/cm^3	

CHAPTER IV

MAGNETOCRYSTALLINE ANISOTROPY

Introduction

The magnitude of the magnetocrystalline anisotropy (hereafter referred to as anisotropy) is measured by the anisotropy energy, which is the work required to rotate the magnetization from the easy crystallographic direction to the hard direction. For a hexagonal material such as $SmCo_5$, the anisotropy can be expressed in terms of anisotropy constants in either of two ways,

$$(9) \quad E_A = K_0 + K_1 \sin^2\theta + K_2 \sin^4\theta + \ldots$$

and

$$(10) \quad E_A = k_2 Y_2^0(\theta,\emptyset) + k_4 Y_4^0(\theta,\emptyset) + k_6 Y_6^0(\theta,\emptyset) + \ldots ,$$

where θ is the angle between the c-axis and the saturated moment, $\emptyset$ is the angle between an a-axis and the saturated moment and $Y_\ell^m(\theta,\emptyset)$ are normalized spherical harmonics. Eq. (9) is based on a series of even powers of $\sin\theta$ and is used commonly because of its mathematical simplicity. Eq. (10) more nearly reflects the true physical picture since spherical harmonics are the appropriate function to describe the energy density on the surface of a sphere. Eq. (10) is generally used in any theoretical consideration of anisotropy. The relationships between the two types of anisotropy constants are

$$(11) \quad K_0 = k_2 + k_4 + k_6$$

$$K_1 = -(1.5k_2 + 8k_4 + 10.5k_6)$$

$$K_2 = 4.375k_4 + 23.625k_6 \qquad \text{(reference 32)}.$$

29

The terms listed in eqs. (9) and (10) are independent of $\emptyset$ and, therefore, represent cylindrical symmetry, not hexagonal symmetry. In general, any $Y_\ell^m(\theta,\emptyset)$ where $m=0$ is independent of $\emptyset$. Basal plane anisotropy is given by higher order terms in eqs. (9) and (10), but basal plane anisotropy is not relevant to this discussion. For most RCo_5 compounds, the anisotropy can be completely described by the terms listed in eqs. (9) and (10).

The relative and absolute values of the anisotropy constants can predict certain types of magnetic behavior. For example, by finding the minima of the anisotropy energy with respect to angle θ, the easy direction(s) can be determined. The results of this calculation are shown in Fig. 9 for K_1 and K_2 and in Fig. 10 for k_2 and k_4. In $SmCo_5$, K_1 is positive ($\sim 10^8$ erg/cm^3) and $K_2 = 0$, therefore, the c-axis is the easy direction.

A good permanent magnet material has an easy axis rather than an easy cone or easy plane. A material with an easy axis has the potential for a large coercivity since a large amount of work, in the form of a large reverse magnetic field, is required to rotate the magnetization through 180°. This is not the case for an easy plane material where little or no work is required to rotate the magnetization in the plane. The easy cone is an intermediate case. Less work is required to reverse the magnetization in an easy cone material than in an easy axis material. Therefore, easy plane materials and most easy cone materials are not suitable permanent magnet materials.

For a material to show anisotropy or magnetostriction, the atomic

K_1

$K_2 = -K_1$

EASY
AXIS

K_2

EASY
PLANE

EASY
CONE

$K_2 = \dfrac{|K_1|}{2}$

$\theta = \sin^{-1}\left(-\dfrac{K_1}{2K_2}\right)^{1/2}$
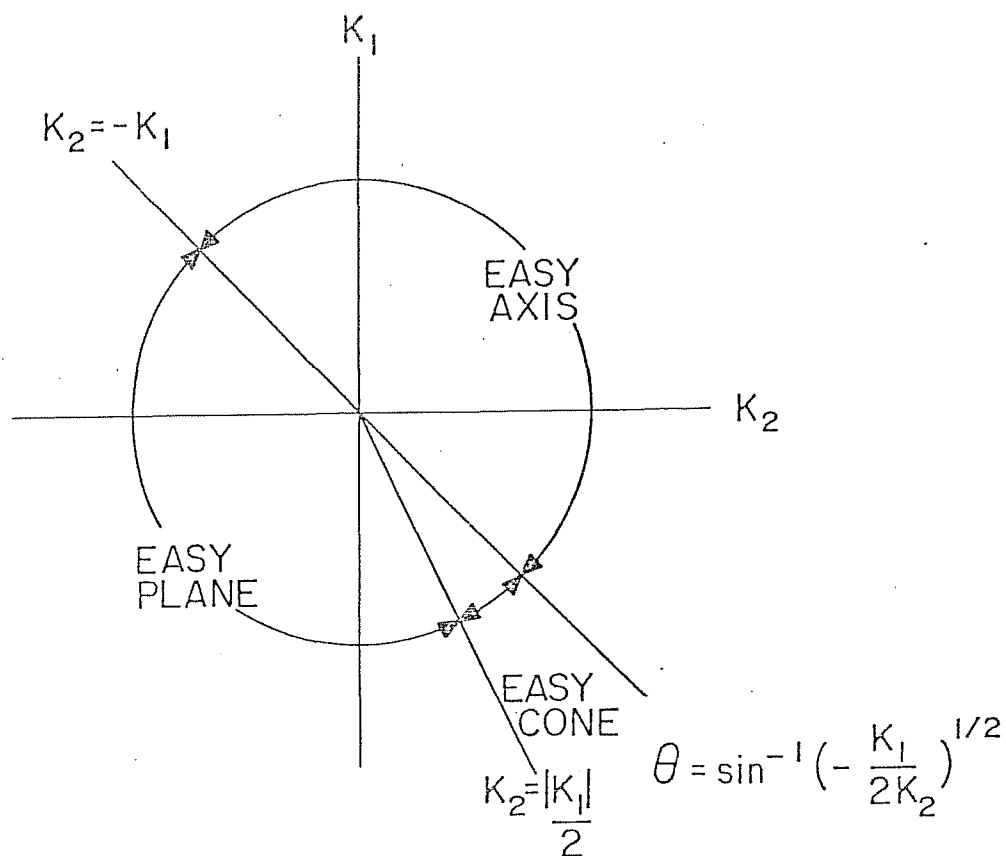
Fig. 9. Easy directions for combinations of K_1 and K_2.
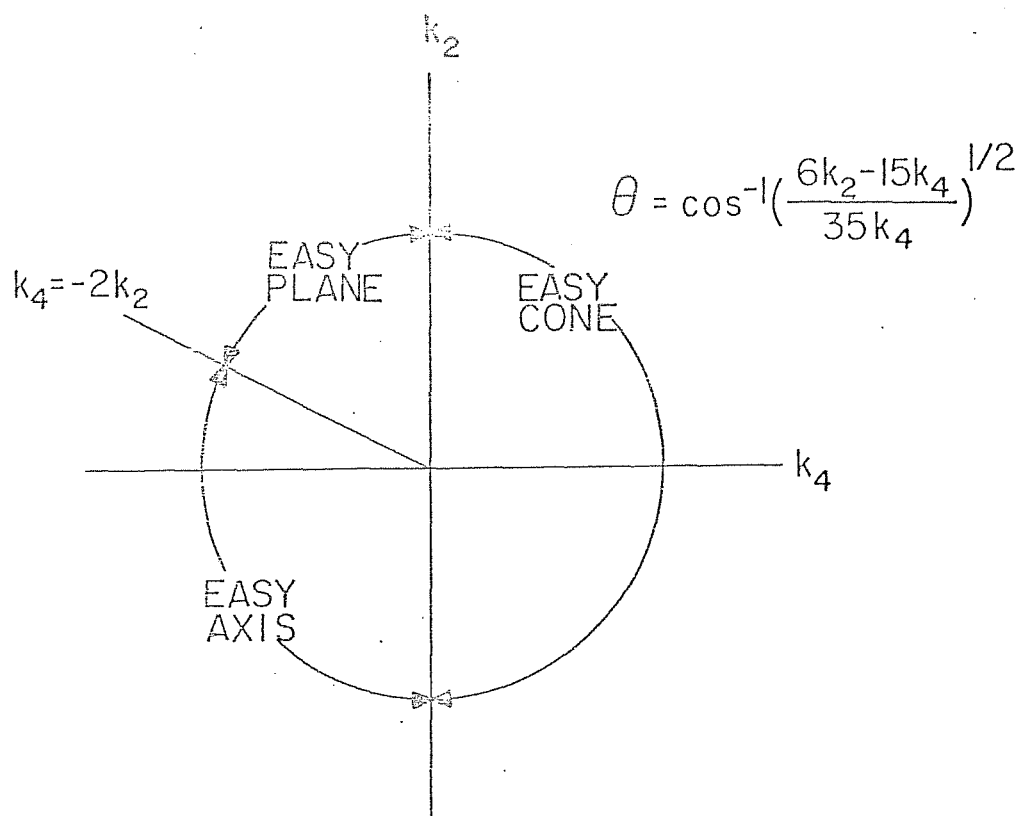
Fig. 10. Easy directions for combinations of k_2 and k_4.

moments must interact with the crystal lattice. However, the spins do not interact directly with the lattice. A mechanism to couple spin moments to the lattice is spin-orbit coupling in a crystal electric field. In ferromagnetic materials, there are partially filled inner electron shells. These are 3d electrons in transition metals and 4f electrons in rare earth metals. The unfilled shells produce nonspherical electron clouds. The orbiting of the inner shell electrons around the nucleus at relativistic speeds causes the coupling of the electron spin moment to the electron orbital moment. Spin-orbit coupling is generally stronger in rare earth metals since the 4f electrons are closer to the nucleus and orbit at a faster rate. The crystal electric field, arising from the neighboring ions, tends to align the orbital moment, and the spin moment by spin-orbit coupling, along a favored crystallographic direction. When a magnetic field is applied to a ferromagnetic material, the moments and the electron clouds rotate to orient themselves with the field. The work required to rotate the moments is the anisotropy. The dimensional change that accompanies the rotation of nonspherical electron clouds is the magnetostriction. In transition metals, the anisotropy is small, 10^3-10^5 erg/cm^3, however, in the rare earth metals and compounds, the anisotropy can be quite large, 10^6-10^8 erg/cm^3.

A simple model to explain the temperature dependence of the anisotropy was proposed by Zener.[33] This model was partially successful in explaining the temperature dependence of the anisotropy by considering the effect of thermal vibrations on each moment and

treating the model as a random walk problem. There are two main
assumptions in Zener's approach. First, the sole effect of tempera-
ture is to introduce fluctuations in the direction of the local
moment. Furthermore, the magnitude of the local moment is independ-
ent of temperature and eqs. (9) and (10) are assumed to represent
the local anisotropy energy density. Second, the deviation in the
direction of the local moment from the easy axis is the result of a
large number of very small deviations having independent random
directions. The effect of temperature on the anisotropy is sche-
matically represented in Fig. 11. The solid curve represents the
intrinsic anisotropy energy which is also the macroscopic anisotropy
energy at T = 0 K. The dotted curve represents the macroscopic
anisotropy energy at a temperature above 0 K. The thermal energy
causes the moment to vibrate, increasing the anisotropy energy
parallel to the easy axis and decreasing the anisotropy energy
perpendicular to the easy axis. Thus as the temperature increases,
the anisotropy decreases. Using this model, Zener predicted that
the anisotropy constants (k_ℓ from eq. (10) where ℓ = 2, 4, 6, ...)
should vary as the $\frac{1}{2}\ell(\ell + 1)$ power of the reduced saturation magnet-
ization, $M_S(T)/M_S(T=0) = m(T)$,

$$(12) \quad k_\ell(T) = k_\ell(T=0) \, m(T)^{\frac{1}{2}\ell(\ell + 1)}.$$

The implicit assumption of the Zener model is that each atomic
moment is localized; that is, each moment behaves like a single-ion
in the lattice. The present understanding of the temperature depend-
ence of the anisotropy and the magnetostriction based on the single-

C-AXIS

INTRINSIC ANISOTROPY ENERGY

SATURATION MOMENT, T=0

SATURATION MOMENT, T>0

$K_i(T)$

$K_1(T=0)$

MACROSCOPIC ANISOTROPY ENERGY, T>0
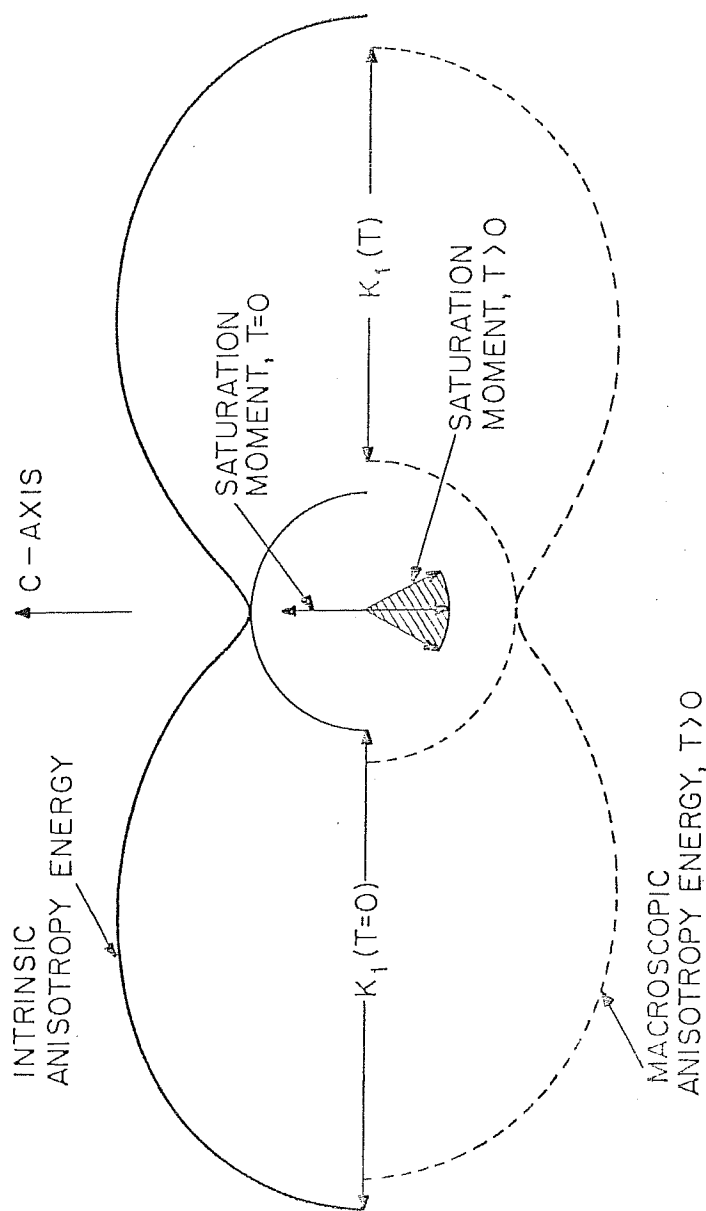
Fig. 11.   Temperature dependence of the anisotropy for an easy axis material with positive K_1 and $K_2=0$, according to the Zener model. The solid curve represents the intrinsic anisotropy energy which is also the macroscopic anisotropy energy at T=0 K. The difference in the anisotropy energy parallel and perpendicular to the c-axis is K_1 at T=0 K. Above 0 K, the saturation moment is thermally excited. The macroscopic anisotropy energy, represented by the dotted curve, is the average of the intrinsic curve over the range of thermal vibrations. This increases the energy parallel to the c-axis and decreases the energy perpendicular to the c-axis. Consequently, K_1 decreases with increasing temperature and K_1 is a function of the saturation magnetization. (reference 34).

ion model is due to Callen and Callen.[24] A historical review of the theories of the temperature dependence of the anisotropy is given in another paper by Callen and Callen.[34] The Callen and Callen theory is based on the symmetry of the crystal lattice, the quantum nature of the magnetic moment of each ion and the assumption that each moment is influenced by a local direction-dependent energy density which can be expressed in terms of spherical harmonics. The equation derived by Callen and Callen for the temperature dependence of the anisotropy is

$$(13) \quad k_\varrho(T) = k_\varrho(T = 0) \; \hat{I}_{\varrho+\frac{1}{2}} \left\{ \hat{I}_{\frac{3}{2}}^{-1}(m) \right\}$$

where $\hat{I}_{\varrho+\frac{1}{2}}$ is a normalized hyperbolic Bessel function. This equation is also valid for the temperature dependence of the magnetostriction. Eq. (13) reduces to the Zener prediction, eq. (12), at low temperatures.

Eq. (13) describes the temperature dependence of the anisotropy and magnetostriction of rare earth metals very well since the 4f electrons are close to the nucleus and considered localized. However, eq. (13) does not work well with transition metals where the 3d electrons are itinerant or nonlocalized. In principle, the magnitude and temperature dependence of the anisotropy of transition metals may be more accurately described by band theory, although they are unresolved in detail.

In $SmCo_5$, the anisotropy is determined by contributions from the cobalt sublattice and the samarium sublattice. The cobalt sublattice contributes a positive K_1 which favors an easy axis. This contribution dominates the anisotropy at room temperature and above. The rare earth contribution dominates the anisotropy below room temperature.[35] This can change the sign of K_1 with decreasing temperature

as in $NdCo_5$ and $PrCo_5$ as shown by Tatsumoto et al.[10]

In a strict sense, the Callen and Callen theory should not necessarily apply to $SmCo_5$ because the cobalt electrons are delocalized. However, the temperature dependence of the anisotropy and magnetostriction may follow eq. (13) if the samarium contribution to the anisotropy is dominant or if the cobalt contribution is not greatly different from the single-ion model. One might expect the temperature dependence of the anisotropy and magnetostriction to follow eq. (13) below room temperature where the samarium contribution to the anisotropy is largest. A modified single-ion model has been successfully used to estimate the magnitude and temperature dependence of the anisotropy of $SmCo_5$.[36]

Experiment

Two methods have been used in previous studies to measure the anisotropy constants of $SmCo_5$: the approach to saturation method and the torque magnetometer.

To measure the anisotropy constants by the approach to saturation method, magnetization curves are measured parallel and perpendicular to the easy axis. Typical curves for this measurement are shown in Fig. 12 for $SmCo_5$. Following the argument used by Cullity,[37] the anisotropy constants are determined by the shape of the magnetization curve measured perpendicular to the easy axis. See Fig. 13 for measurement orientations. The magnetic potential energy for the hard axis case is

$$(14) \quad E_p = -M_s H \cos(90 - \theta).$$

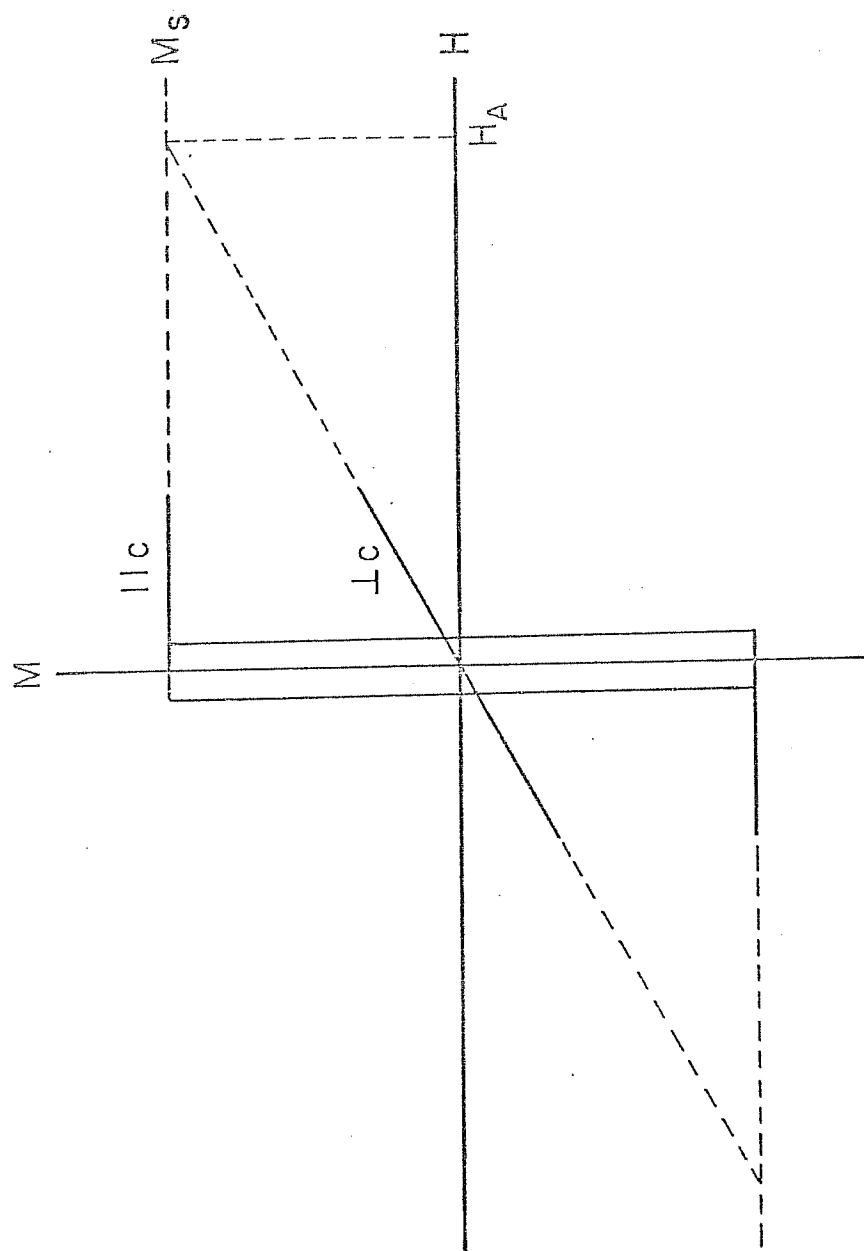Fig. 12. Approach to saturation method, magnetization curves parallel and perpendicular to the c-axis for $SmCo_5$.
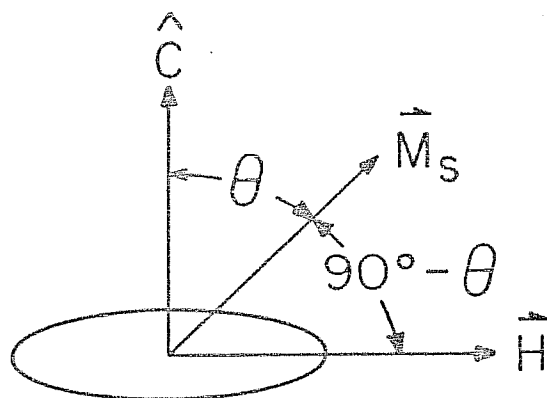
Fig. 13. Relationship of c-axis, M_s and applied field when the magnetization is measured perpendicular to the c-axis.

The position of the saturated moment is determined by the minimum of the potential and anisotropy energies. Using eq. (9) for the anisotropy energy gives,

$$(15) \quad \frac{\partial}{\partial \theta}(E_A + E_p) = 2K_1 \sin\theta \cos\theta + 4K_2 \sin^3\theta \cos\theta$$
$$- M_s H \cos\theta = 0$$
$$\text{or} \quad 2K_1 \sin\theta + 4K_2 \sin^3\theta = M_s H.$$

The component of the magnetization parallel to the applied field is

$$(16) \quad M = M_s \sin\theta.$$

Combination of eqs. (15) and (16) to eliminate θ yields

$$(17) \quad H = (M/M_s) \, 2K_1/M_s + (M/M_s)^3 \, 4K_2/M_s.$$

The field required to saturate the sample in the hard direction is

$$(18) \quad H = (2K_1 + 4K_2)/M_s.$$

Knowing the saturation magnetization from the easy axis measurement and the shape of the hard axis magnetization curve, the anisotropy constants can be determined by fitting eq. (17) to the experimental data. If $K_2 = 0$, the field in eq. (18) is the anisotropy field, $H_A = 2K_1/M_s$.

Alternatively, the hard axis magnetization curve can be replotted as an H/M vs. M^2 curve. In this representation, the slope of the curve is $4K_2/M_s^2$ and the intercept is $2K_1/M_s^2$. This result follows directly from eq. (17) and was first derived by Sucksmith and Thompson.[38]

Another way to measure the anisotropy constants is to measure the torque acting on a single crystal or aligned powder in a magnetic field, using a torque magnetometer. The general relationship between

the sample axis, the magnetization and the applied field is shown in Fig. 14. A plot of torque against angle ψ can be measured by rotating either the field or the sample. As Fig. 14 shows, the magnetization and applied field are generally not parallel. The position of the saturated moment in the sample is determined by balancing the torque due to anisotropy and the torque from rotating the saturated moment away from the applied field. These torques are given by

$$(19) \quad L_A = -\frac{\partial E_A}{\partial \theta} = -2 K_1 \sin\theta \cos\theta - 4 K_2 \sin^3\theta \cos\theta$$

$$= -(K_1 + K_2) \sin 2\theta + \tfrac{1}{2} K_2 \sin 4\theta$$

and

$$(20) \quad L_{MH} = H M_S \sin(\psi - \theta),$$

respectively. In a nonaccelerating sample, the torques sum to zero,

$$(21) \quad H M_S \sin(\psi - \theta) = (K_1 + K_2) \sin 2\theta - \tfrac{1}{2} K_2 \sin 4\theta = L.$$

Since the sample is rigidly attached to the sample holder, the measured torque is actually the torque acting on the c-axis of the sample, which also equals L. This torque is balanced by the mechanical torque on the sample holder.

The torque magnetometer used in this experiment is shown in Fig. 15. The torque is sensed by four strain gages mounted in perpendicular pairs, at 45 degrees to the axis of rotation on opposite sides of a brass cylinder. The strain gages are connected as the arms of a Wheatstone Bridge in the measuring circuit shown in Fig. 16. The angle ψ is measured by a gear driven 10-turn potentiometer at the top of the torque magnetometer. The temperature is measured by a copper-constantan thermocouple mounted less than 5 mm from the sample.
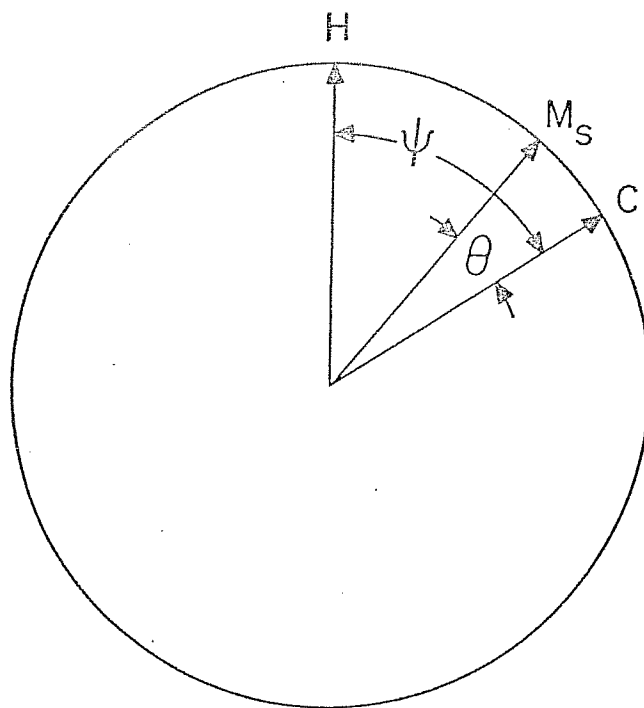
$$L = -(K_1 + K_2) \sin 2\theta + \frac{1}{2} K_2 \sin 4\theta$$

$$= - M_S H \sin(\psi - \theta)$$

Fig. 14. Relationship of the sample c-axis, the applied field
and the rotated saturation magnetization in the
torque sample. Equations give the magnitude of the
measured torque.

MOTOR

ANGLE SENSING POT

BEARING

LEVEL ADJUSTMENT

POSITION ADJUSTMENT

STRAIN GAGES

STAINLESS STEEL TUBE

THERMOCOUPLE

CLAMPING SCREW

SAMPLE

MAGNET WINDINGS

TAPERED IRON POLE PIECES

FULL SCALE CROSS SECTIONAL VIEW

Fig. 15.   Torque magnetometer.

Fig. 16. Torque measuring circuit.

Typically, the period of rotation was about 20 seconds.

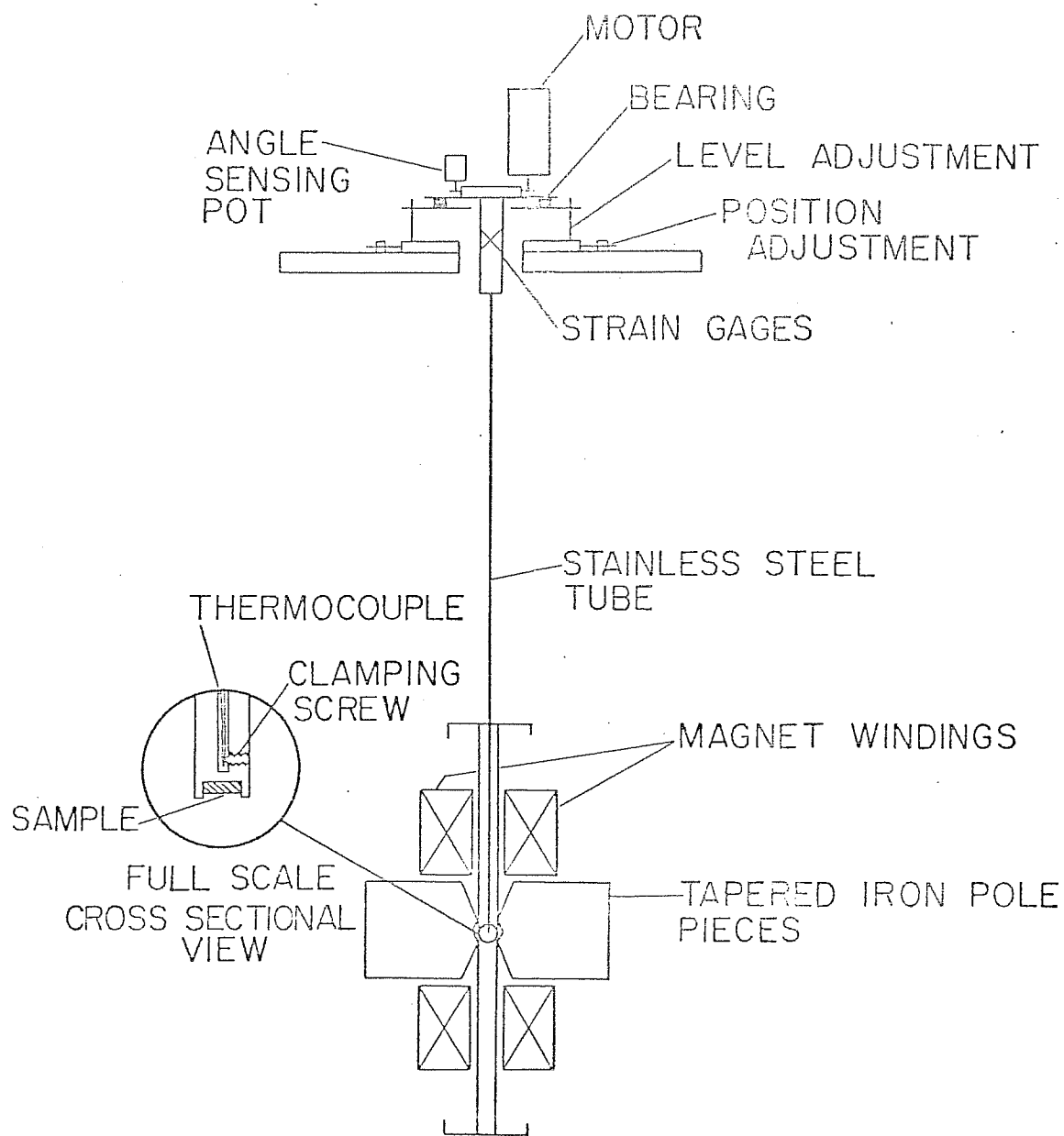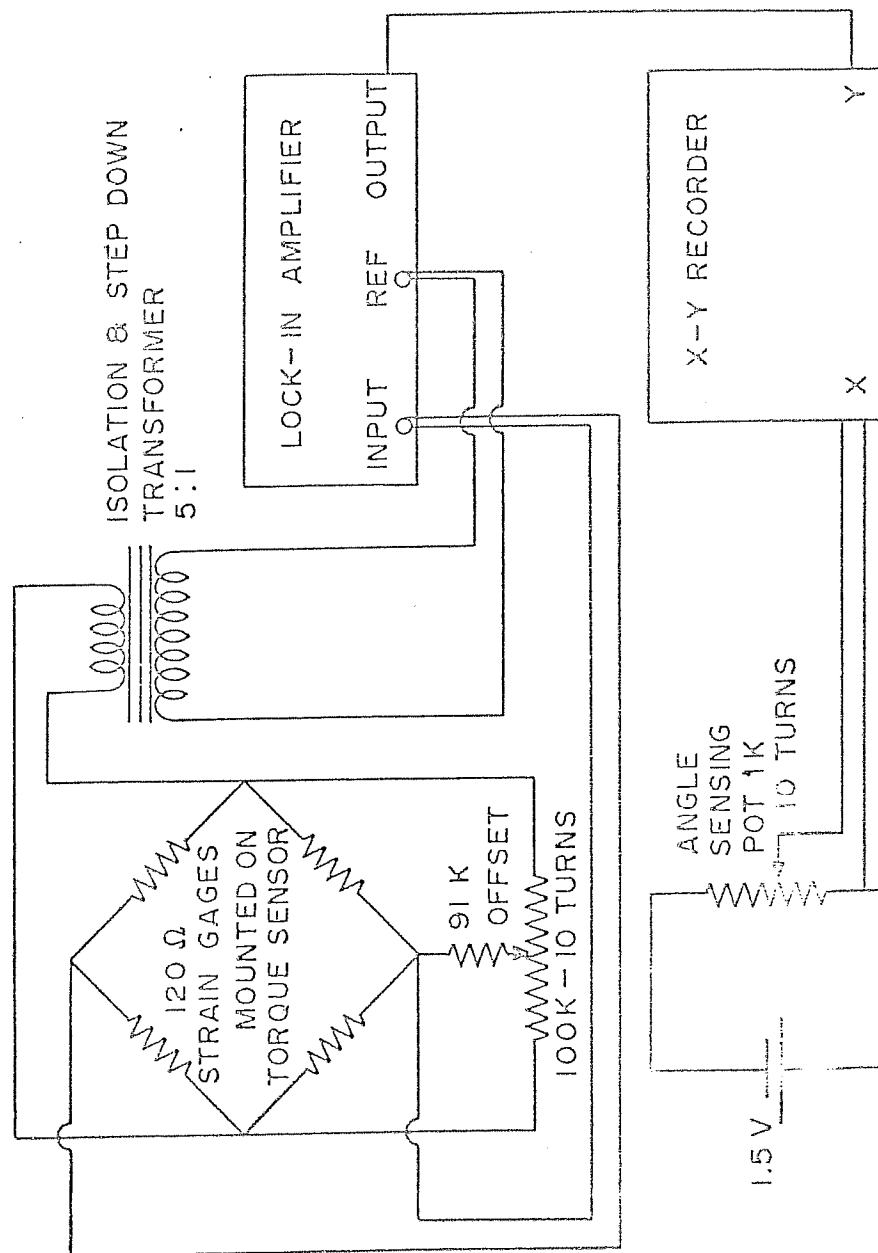A torque curve of an $SmCo_5$ single crystal measured at 302 K with an applied field of 65630 Oe is shown in Fig. 17. Note the sharp discontinuities at $\Psi = 90^\circ$ and 270°. Near these angles, it becomes energetically favorable for the sample to divide into domains. The torque changes rapidly as the domain walls travel through the sample, reversing the direction of the magnetization. The hysteresis is due to the coercive field of the sample and the limited response of the X-Y recorder and the Lock-In amplifier when there is a sharp change in signal. Reducing the sweep speed was found to decrease the hysteresis. Since the observed torque in this region is controlled by the demagnetization of the sample and the response of the instrumentation, this part of the torque curve is not used to determine the anisotropy constants.

The anisotropy constants can be determined by finding the slope of the torque curve at two points. To find K_1, the slope is measured at $\Psi = 0$. Using eq. (20) the slope and K_1 are related by

$$(22) \quad K_1 = \frac{\frac{1}{2} \left(\frac{\partial L}{\partial \Psi} \right)_{\Psi = 0}}{1 - \frac{1}{H M_s} \left(\frac{\partial L}{\partial \Psi} \right)_{\Psi = 0}}$$

To find K_2, the slope is taken at another point on the curve. This technique yields an uncertain value for the anisotropy constant. Since only one point on the torque curve is used to find K_1 and the denominator of eq. (22) is very small, any errors in H, M_s and $(\partial L / \partial \Psi)_{\Psi = 0}$ are magnified.

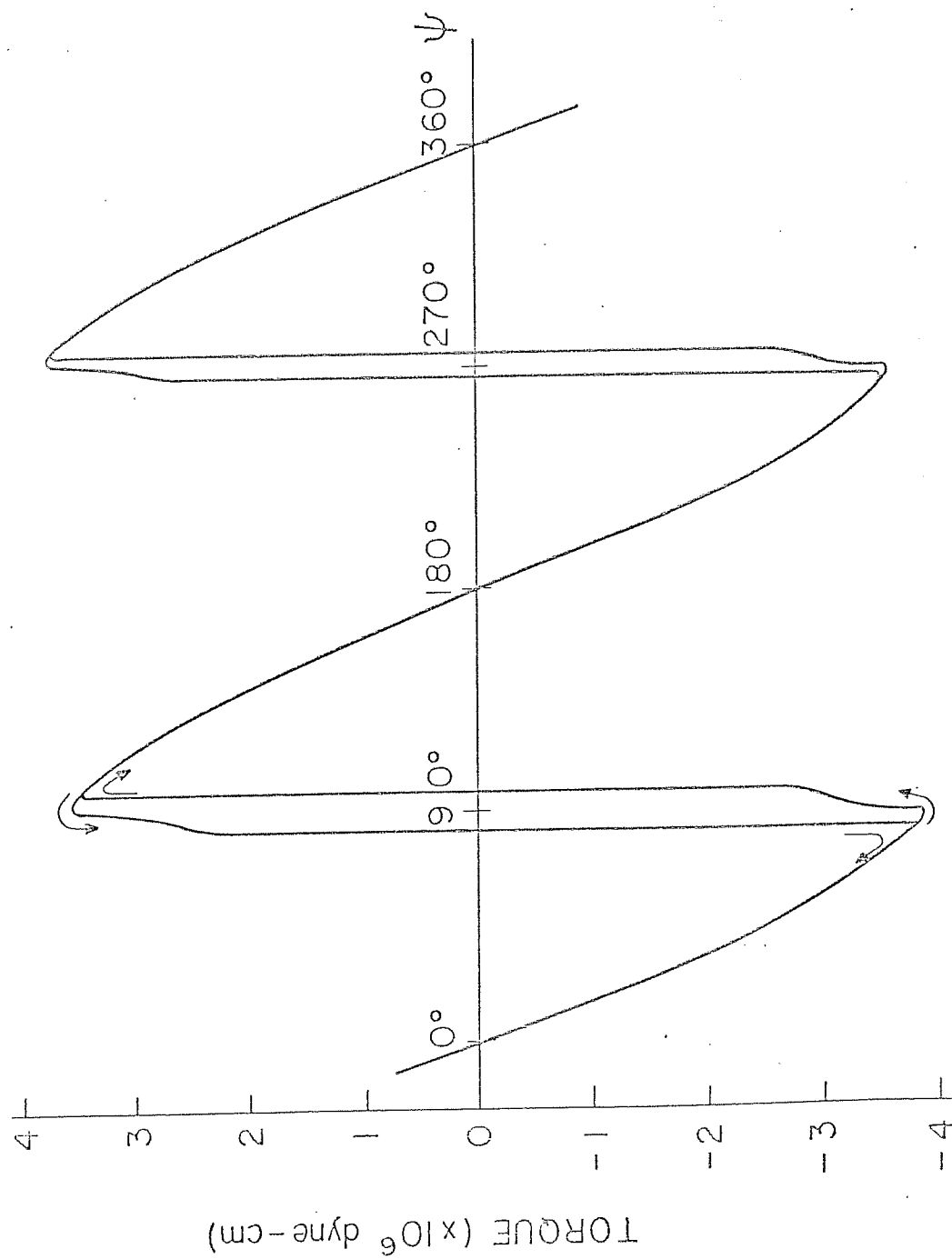Alternatively, a computer aided fitting scheme can be employed

Fig. 17. Typical torque curve for SmCo$_5$ single crystal, H = 65.6 kOe and T = 302 K.

using eq. (21) to find the value of K_1 that gives the best fit to the experimental torque curve. The program used to determine K_1 and K_2 is listed in Program I and is briefly described by the following. The torque is recorded at fifteen points on the torque curve. These points are evenly spaced in ψ and all in one period of the curve. The measured ψ is corrected for the slight twisting, less than 1 degree, of the stainless steel tube. For each curve, the applied field, temperature and saturation magnetization are known. The only unknowns in eq. (21) are K_1, K_2 and θ. Initially, K_2 is ignored. For each trial value of K_1, θ is calculated by solving

$$(23) \quad K_1 \sin 2\theta = M_s H \sin (\psi - \theta),$$

for each data point. Using the calculated θ, a torque is calculated. For each K_1, there is a calculated torque curve. The value of K_1 is found that gives the best agreement between calculated and experimental torque curves. Once a value for K_1 is established, values for K_2 can be examined using the same approach. However, the addition of K_2 to the analysis does not significantly improve the fit of the calculated and experimental curves. Therefore, within the accuracy of this experiment, $K_2 = 0$. This is not unexpected since the calculated θ values are very small. At the largest angles measured, $\psi = 75$ degrees, θ was only 6 degrees at 4.2 K and 11 degrees at 410 K. Any effect from K_2 is nearly impossible to detect at such small angles.

Results

The K_1 vs. T data from this analysis are plotted in Fig. 18

```
100 REM PROGRAM TO HANDLE TORQUE DATA
110 DIM X(30),Y(30),Z(30),L(30),K(30)
115 REM X(I) IS THE MEASURED ANGLE
116 REM Y(I) IS X(I) CORRECTED FOR THE TWIST IN THE SHAFT
118 REM Z(I) IS THE ANGLE BETWEEN THE C-AXIS AND THE MAGNETIZATION
150 READ N,H,X,Y,X(1),D,M,S,T
155 REM N=# OF DATA PTS.,H=FIELD,X=KAL/CM,Y=TORQUE(C.CM),X(1)=STARTING ANGLE
160 REM D=INCREMENT,M=MASS,S=SATURATION(EMU/G),T=TEMPERATURE
170 X(0)=X(1)*X-D*X
180 V=(1+2.91900E-05*T)*M/8.559/(1+2.91900E-05*300)
190 R=S*M/V
192 REM R=SATURATION(EMU/CM^3),V=VOLUME
200 FOR I=1 TO N
210 READ Y1
220 L(I)=Y*Y1
230 X(I)=X(I-1)+D*X
240 Y(I)=X(I)-4.38000E-09*L(I)
250 Z(I)=Y(I)-ATN(L(I)/SQR((H*S*M)^2-L(I)^2))
270 PRINT Y1,L(I),X(I),Y(I),Z(I)
290 NEXT I
300 FOR K1=1.00000E+08 TO 4.00000E+08 STEP 5.00000E+07
310 GOSUB 1000
320 NEXT K1
400 PRINT "RANGE FOR K1";
405 INPUT H1,H2,H3
410 FOR K1=H1 TO H2 STEP H3
420 GOSUB 1000
430 NEXT K1
490 OPEN "KB:" FOR OUTPUT AS FILE #1 DOUBLE BUF
500 PRINT "VALUE FOR K1";
505 INPUT K1
510 GOSUB 2000
530 PRINT #1;"GOODNESS OF FIT =";SQR(S1/N)
540 PRINT #1
550 CLOSE #1
560 GO TO 490
600 FOR K2=-K1/2 TO K1/2 STEP K1/10
620 GOSUB 2500
640 NEXT K2
900 DATA 15,65630
901 DATA .374,567000,-3.5,.5
905 DATA .5613
910 DATA 95.3,410
920 DATA -5.63,-4.93,-4.29,-3.66,-2.91,-2.01,-1.11,-.11
930 DATA .94,1.89,2.89,3.79,4.44,5.04,5.44
999 END
1000 REM SUBROUTINE TO CALCULATE GOODNESS OF FIT
1005 S1=0
1010 FOR I=1 TO (N-1)/2
1020 GOSUB 1500
1160 Z(I)=Z
1170 S1=S1+(L(I)-V*K1*SIN(2*Z))^2+(L(N+1-I)+V*K1*SIN(2*Z))^2
1180 NEXT I
1190 PRINT K1,SQR(S1/N)
1200 RETURN
1500 REM SUBROUTINE TO DETERMINE THETA
1505 Z=Z(I)
1510 Z=Z+.02
1520 IF K1*SIN(2*Z)-H*R*SIN(Y(I)-Z)<0 THEN 1510
1530 Z=Z-.01
1540 IF K1*SIN(2*Z)-H*R*SIN(Y(I)-Z)>0 THEN 1530
1550 Z=Z+1.00000E-03
1560 IF K1*SIN(2*Z)-H*R*SIN(Y(I)-Z)<0 THEN 1550
```

```
1570 Z=Z-1.00000E-04
1580 IF K1*SIN(2*Z)-H*R*SIN(Y(I)-Z))0 THEN 1570
1590 Z=Z+1.00000E-05
1600 IF K1*SIN(2*Z)-H*R*SIN(Y(I)-Z)<0 THEN 1590
1610 Z=Z-1.00000E-06
1620 IF K1*SIN(2*Z)-H*R*SIN(Y(I)-Z))0 THEN 1610
1630 Z=Z+5.00000E-07
1640 RETURN
2000 S2=0
2005 S1=0
2010 PRINT #1;N,H,X,Y,X(1)
2015 PRINT #1;
2020 PRINT #1;D,M,S,R,V
2025 PRINT #1;
2030 PRINT #1;"TEMPERATURE =";T;"K","K1 =";K1
2035 PRINT #1;
2040 PRINT #1;"PSI","EXP L","CALC L","ERROR","THETA"
2045 FOR I=1 TO N
2050 GOSUB 1500
2100 S1=S1+(L(I)-V*K1*SIN(2*Z))^2
2190 E=0
2195 IF I=(N+1)/2 THEN 2204
2200 E=(L(I)-K1*SIN(2*Z)*V)/L(I)
2203 S2=S2+ABS(E)/N
2204 PRINT #1;INT(Y(I)*5729.58+.5)/100,L(I),K1*V*SIN(2*Z),;
2205 PRINT #1;INT(E*10000+.5)/100,INT(Z*5729.57+.5)/100
2210 NEXT I
2220 PRINT #1;
2250 PRINT #1;"AVERAGE ERROR =";INT(S2*10000+.5)/100;"%"
2260 PRINT #1;
2300 RETURN
2500 REM SUBROUTINE TO DETERMINE THETA INCLUDING K2
2505 S1=0
2510 FOR I=1 TO N
2520 Z=Z(I)
2530 Z=Z+.02
2540 IF (K1+K2)*SIN(2*Z)-.5*K2*SIN(4*Z)-H*R*SIN(Y(I)-Z)<0 THEN 2530
2550 Z=Z-.01
2560 IF (K1+K2)*SIN(2*Z)-.5*K2*SIN(4*Z)-H*R*SIN(Y(I)-Z))0 THEN 2550
2570 Z=Z+1.00000E-03
2580 IF (K1+K2)*SIN(2*Z)-.5*K2*SIN(4*Z)-H*R*SIN(Y(I)-Z)<0 THEN 2570
2590 Z=Z-1.00000E-04
2600 IF (K1+K2)*SIN(2*Z)-.5*K2*SIN(4*Z)-H*R*SIN(Y(I)-Z))0 THEN 2590
2610 Z=Z+1.00000E-05
2620 IF (K1+K2)*SIN(2*Z)-.5*K2*SIN(4*Z)-H*R*SIN(Y(I)-Z)<0 THEN 2610
2630 Z=Z-1.00000E-06
2640 IF (K1+K2)*SIN(2*Z)-.5*K2*SIN(4*Z)-H*R*SIN(Y(I)-Z))0 THEN 2630
2650 Z=Z+5.00000E-07
2700 Z(I)=Z
2710 S1=S1+(L(I)-V*H*R*SIN(Y(I)-Z))^2
2720 NEXT I
2730 PRINT K2,SQR(S1/N)
2740 RETURN
3000 STOP
```
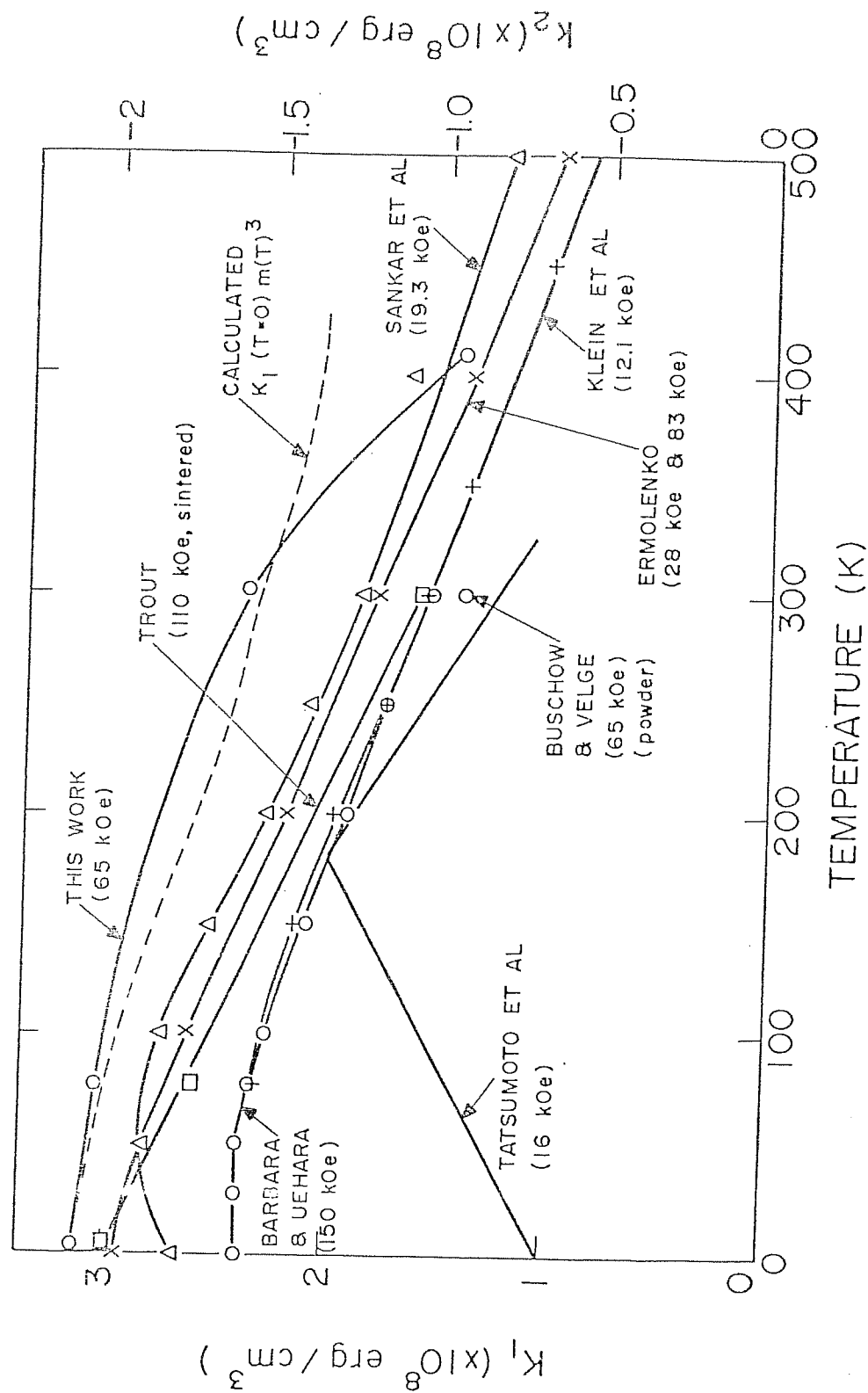
Fig. 18. Anisotropy vs. temperature for this work and other studies. The maximum applied field used in each study is given in parenthesis.

and are compared to the results of earlier experiments. The largest
applied field in each experiment is shown in parenthesis. All
previous studies used the approach to saturation method except Klein
et al.[29] who used a torque magnetometer. Ermolenko[30] used the torque
method with a maximum applied field of 28 kOe at room temperature
and above and the approach to saturation method with a maximum field
of 83 kOe below room temperature. All earlier experiments used bulk
$SmCo_5$ single crystals except for Buschow and Velge[21] who used an
aligned powder sample.

In addition to the data at fixed temperatures reported here,
torque curves were taken continuously as the sample warmed from 4.2 K
to nearly room temperature to see if there is a peak in K_1 as noted
by Tatsumoto et al.[10] and to a lesser extent by Sankar et al.[39] This
experiment showed that no such peak exists; K_1 decreases monotoni-
cally with increasing temperature. The observed peaks in references
10 and 39 are probably due to the low fields used to measure the
anisotropy.

The estimated uncertainty for the K_1 values is $\pm$ 25% at 4.2 K
and $\pm$ 10% at 410 K. The error is estimated by varying an input
value for the saturation magnetization, mass or torque calibration
by $\pm$ 3%. The value $\pm$ 3% is chosen to represent the total error of
all the data put into the computer program. The change in K_1 caused
by the intentional variation of the input data gives an estimate of
the uncertainty of the anisotropy measurement. A small error in any
of the measured quantities that are used to determine K_1 will cause a

large uncertainty in K_1. All measurements of the anisotropy of $SmCo_5$ have this problem regardless of the method used. The fundamental problem is that $SmCo_5$ cannot be saturated perpendicular to the c-axis with any available field at temperatures of interest. To find K_1, one must observe the behavior of the saturated moment as it rotates over a small angle in θ, either by measuring the torque or the magnetization. In either case, a small error in the measurement causes a large error in the determination of K_1. Also it is difficult to determine if there is a K_2 at such small angles.

The error in the approach to saturation method depends on the maximum available field, the measured anisotropy and the accuracy in measuring magnetization. The error is given by

$$(24) \quad e = e_{mag} (1 + 2K_1/M_s H_{max})$$

where e_{mag} is the error in the measured magnetization and H_{max} is the maximum available field. If e_{mag} = 2 %, the calculated range of errors for Sankar et al.[39] is 32 % at 500 K and 65 % at 50 K, and for Barbara and Uehara,[40] the range is 7 % at 300 K and 9 % at 0 K. If the accuracy of the magnetization measurement is better, if e_{mag} = 1 %, the above errors would be cut in half. This calculation shows the need for using the highest available fields and the most accurate measurement of magnetization.

Within the accuracy of the experiment, the results agree with most previous results: Barbara and Uehara,[40] Sankar et al.,[39] Ermolenko[30] and Klein et al.[29] However, the K_1 values reported here are the largest ever reported for $SmCo_5$.

Fig. 18 also compares this measurement to the Callen and Callen theory for the temperature dependence of the anisotropy.[24] Since K_1 is the only nonzero anisotropy constant in eq. (9), eq. (12) is equivalent to

$$(25) \quad K_1(T) = K_1(T=0) \; m(T)^3.$$

To apply eq. (25) to a compound, the saturation magnetization of each sublattice must be considered separately. Since the Sm moment is much smaller than the Co moment and there is uncertainty about the value of the Sm moment, the simplest approach is to use the total moment. If this were not the case, it would be necessary to find the temperature dependence of each sublattice. This could be accomplished by comparing the measured temperature dependence of the saturation magnetization of $SmCo_5$ with YCo_5; a compound with the same crystal structure and where the Y^{+3} ion has no magnetic moment.

Below 425 K, eqs. (12) and (25) are an excellent approximation for eq. (13); the maximum error is less than 0.5%. Eq. (25) is plotted as a dashed line in Fig. 18. There is good agreement between the Callen and Callen theory prediction and the measured data below 300 K. It is in this region where the samarium contribution to the anisotropy is greatest.

There is also good agreement with some earlier anisotropy measurements on sintered $SmCo_5$ permanent magnets.[41] Since the sintered magnets are not perfectly aligned and are slightly off the stoiciometric composition, K_1 for the sintered magnets is lower than the single crystals.

MAGNETOSTRICTION

Theory

Magnetostriction is a dimensional change in a substance due to an applied magnetic field. As mentioned in Chapter IV, magneto-striction arises from spin-orbit coupling in a crystal electric field. The rotation of nonspherical electron clouds in a magnetic field causes the strains associated with magnetostriction. As in the case of anisotropy, magnetostriction is a small effect in transition metals, 10^{-5}-10^{-4}, and larger in rare earth metals and compounds, 10^{-4}-10^{-2}.

Four magnetostriction constants are usually required to describe the magnetoelastic deformation in a hexagonal material. There are two ways to write the magnetostrictive strains in this case,

$$(26) \quad \lambda_{si} = \lambda_A \left[(\alpha_1\beta_1 + \alpha_2\beta_2)^2 - (\alpha_1\beta_1 + \alpha_2\beta_2)\alpha_3\beta_3 \right]$$
$$+ \lambda_B \left[(1 - \alpha_3^2)(1 - \beta_3^2) - (\alpha_1\beta_1 + \alpha_2\beta_2)^2 \right]$$
$$+ \lambda_C \left[(1 - \alpha_3^2)\beta_3^2 - (\alpha_1\beta_1 + \alpha_2\beta_2)\alpha_3\beta_3 \right.$$
$$+ 4\lambda_D (\alpha_1\beta_1 + \alpha_2\beta_2)\alpha_3\beta_3$$

and

$$(27) \quad \lambda_{si} = \left[\lambda_1^{\alpha,0} + \lambda_1^{\alpha,2}(\alpha_3^2 - \tfrac{1}{3}) \right] (\beta_1^2 + \beta_2^2)$$
$$+ \left[\lambda_2^{\alpha,0} + \lambda_2^{\alpha,2}(\alpha_3^2 - \tfrac{1}{3}) \right] \beta_3^2$$
$$+ \tfrac{1}{2}\lambda^{\delta,2} \left[(\alpha_1\beta_1 + \alpha_2\beta_2)^2 - (\alpha_1\beta_1 + \alpha_2\beta_2)^2 \right]$$
$$+ 2\lambda^{\epsilon,2} (\alpha_1\beta_1 + \alpha_2\beta_2)\alpha_3\beta_3.$$

Eq. (26) is due to Mason[42] and is a phenomenological equation based

54

on a general thermodynamic function and hexagonal symmetry. Eq. (27)
is due to Clark et al.[32] and is derived from a magnetoelastic
Hamiltonian with hexagonal symmetry. In both equations, α and β
are the direction cosines of the magnetization and of the direction
of strain measurement, with the orthogonal axis given by the subscript.
The two sets of magnetostriction constants are related by,

$$(28) \quad \lambda^{\gamma,2} = \lambda_A - \lambda_B$$

$$\lambda_1^{\alpha,2} = -\tfrac{1}{2}(\lambda_A + \lambda_B)$$

$$\lambda_2^{\alpha,2} = -\lambda_C$$

$$\lambda^{\epsilon,2} = 2\lambda_D - \tfrac{1}{2}(\lambda_A + \lambda_B) \quad \text{(reference 32)}.$$

The constants $\lambda_1^{\alpha,0}$ and $\lambda_2^{\alpha,0}$ in eq. (27) represent the anomalous thermal
expansion because they are independent of the magnetization.[32] The
axes in eqs. (26) and (27) are orthogonal, not hexagonal, the orthogonal
3-axis coicides with the hexagonal c-axis. Actually, eqs. (26) and (27)
are second order approximations of the magnetostriction in a hexagonal
material. Note that λ_{si} is invariant to an interchange of the 1 and 2
axes which is equivalent to cylindrical symmetry.

As mentioned earlier, magnetostriction and anisotropy are related
phenomena. Based on a single-ion model, Callen and Callen predict
that the magnetostriction and anisotropy should have the same tempera-
ture dependence.[24] Recalling the limitations of applying the Callen
and Callen theory to SmCo$_5$ mentioned in Chapter IV, the temperature
dependence of the magnetostriction may be of the form

$$(29) \quad \lambda(T) = \lambda(T=0) \; m(T)^3,$$

where $\lambda(T)$ represents any of the second order magnetostriction

constants in eq. (27).

Measurements

The magnetostriction was measured using strain gages. Strain gages make use of the change in resistivity that occurs in a strained material. The change in resistance is directly proportional to the strain; the proportionality constant is called the gage factor. The gage factor is about 2 for metal strain gages and over 100 for semiconductor strain gages. The first use of strain gages to measure magnetostriction was in 1947 by Goldman.[43] An excellent review of this technique and the properties of strain gages is given by Gersdorf.[44]

The four measurements used to determine the eq. (26) magneto-striction constants of $SmCo_5$ are described in Table IV. The values of λ_A, λ_B, and λ_C, are obtained directly from the experiments, if θ is known. Since $SmCo_5$ cannot be saturated in any direction other than the c-axis, with the available magnetic fields and for the temperature range of interest, there is no orientation of sample, strain gage and applied field where the measured strain will be propor-tional only to λ_D. Instead, the configuration used gives a strain of

$$(30) \quad \lambda = \tfrac{1}{2}(\lambda_A + \lambda_C) \sin^2\theta + \tfrac{1}{2}(4\lambda_D - \lambda_A - \lambda_C) \sin\theta \cos\theta.$$

For small angles, this reduces to

$$(31) \quad \lambda = \tfrac{1}{2}(4\lambda_D - \lambda_A - \lambda_C) \sin\theta + \tfrac{1}{2}(\lambda_A + \lambda_C) \sin^2\theta$$
$$- \tfrac{1}{4}(4\lambda_D - \lambda_A - \lambda_C) \sin^3\theta .$$

The determination of λ_D is made from the measured strain and the independently determined values of λ_A and λ_C. Notice that the term

TABLE IV

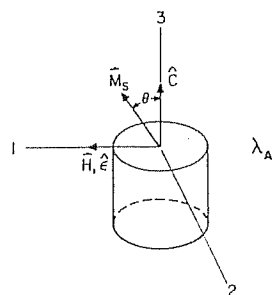| MAGNETOSTRICTION CONSTANT	DIRECTION COSINES OF M_S	DIRECTION COSINES OF STRAIN GAGE	MEASURED STRAIN
λ_A	$\alpha_1 = \sin\theta$ $\alpha_2 = 0$ $\alpha_3 = \cos\theta$	$\beta_1 = 1$ $\beta_2 = 0$ $\beta_3 = 0$	$\epsilon = \lambda_A \sin^2\theta$
λ_B	$\alpha_1 = \sin\theta$ $\alpha_2 = 0$ $\alpha_3 = \cos\theta$	$\beta_1 = 0$ $\beta_2 = 1$ $\beta_3 = 0$	$\epsilon = \lambda_B \sin^2\theta$
λ_C	$\alpha_1 = 0$ $\alpha_2 = \sin\theta$ $\alpha_3 = \cos\theta$	$\beta_1 = 0$ $\beta_2 = 0$ $\beta_3 = 1$	$\epsilon = \lambda_C \sin^2\theta$
λ_D	$\alpha_1 = 0$ $\alpha_2 = -\sin\theta$ $\alpha_3 = \cos\theta$	$\beta_1 = 0$ $\beta_2 = -\sqrt{2}/2$ $\beta_3 = -\sqrt{2}/2$	$\epsilon = \frac{1}{2}(\lambda_A + \lambda_C)\sin^2\theta$ $+ \frac{1}{2}(4\lambda_D - \lambda_A - \lambda_C)$ $\sin\theta\cos\theta$
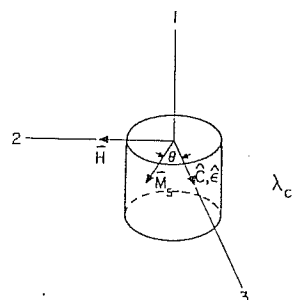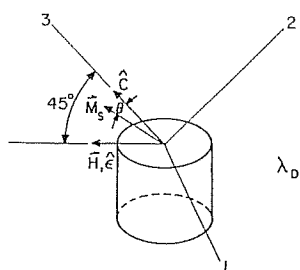
$$(32) \quad \tfrac{1}{2}(4\lambda_D - \lambda_A - \lambda_C) = \lambda^{\epsilon,2}$$

from eq. (28).

Samples of known orientation were mounted on brass sample holders 11 mm in diameter, using M-Bond 43-B epoxy. This epoxy was used because it does not become brittle at low temperatures and it is able to withstand the large torque experienced by the sample in the applied field, as well as the large thermal and magnetostrictive strains of the sample. Micro Measurements WK-13-062AP-350 strain gages were used because of their small size, attached lead wires and low magnetoresistance. The specifications for these gages are shown in Fig. 19. M-Bond 43-B was also used to attach the strain gages to the samples and as a protective coating over the mounted gages.

The assembly for measuring magnetostriction is shown in Fig. 20. The strain gage lead wires were attached to solder tabs mounted on the perimeter of the brass sample holder. Leads from the solder tabs were connected to the measuring circuitry. A lead-tin solder with 1% antimony was used for all connections to prevent the transition of gray tin to brittle white tin at low temperatures. The mounted sample and dummy gage can be independently rotated in the sample mount to any orientation and secured with a set screw. However, the dummy gage was always kept parallel to the sample gage. This arrangement kept both gages in the same thermal and magnetic environment so that any temperature or magnetoresistive effects were balanced out. An experiment with two dummy gages showed the magnetoresistance was less

GENERAL INFORMATION, SERIES WK STRAIN GAGES

GENERAL DESCRIPTION: WK series gages are a family of fully encapsulated K-alloy strain gages used in both experimental stress analysis and transducer application. These gages have integral high-endurance lead ribbons which are completely encapsulated in a matrix consisting of a high-temperature epoxy phenolic resin system reinforced with glass fibers.

TEMPERATURE RANGE: −452 F (−269 C) to +550 F (+290 C) for continuous use in static measurements. Useful to +750 F (+372 C) for short term exposure.

SELF TEMPERATURE COMPENSATION: See data curve below.

STRAIN LIMITS: ±1.5% at room temperature, ±1.0% at −320 F (−195 C), ±3% at +400 F (+205 C).

FATIGUE LIFE: 10⁵ cycles at ±2000 μin/in (μm/m), 10⁷ cycles at ±2200 μin/in (μm/m). Longer gage lengths and lower resistances show greater endurance and less scatter in fatigue life.
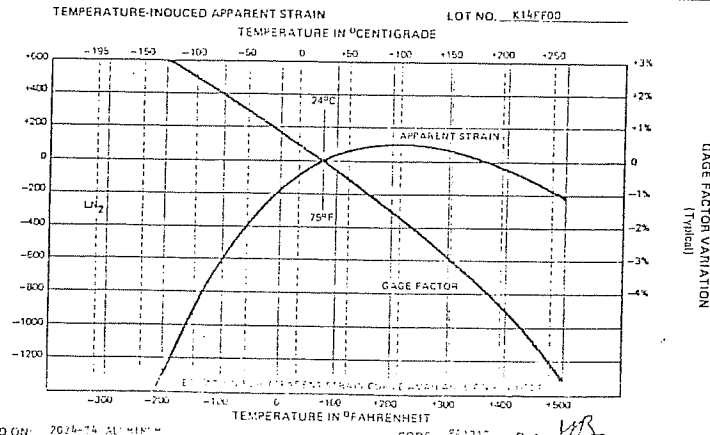
BONDING AGENTS: High temperature epoxy adhesives are recommended for best performance over the entire temperature range. Micro-Measurements M-Bond 610, 600 and M-Bond GA 60 are particularly compatible with WK Series gages. Refer to M-M Bulletin A-142 for information on bonding agents, and B-130 for installation procedures.

LEADWIRE SYSTEM: Two flat high-endurance leads to each tab permit a 3-wire system to be carried directly to the gage, thus eliminating leadwire errors over the wide useful temperature range of the WK Series gages. Option B-87 WK Series gages are supplied with single 0.005 in (0.13 mm) diameter nickel-clad copper wire leads. Option B-129 gages have single 1/32 in (0.8 mm) x 0.002 in (0.05 mm) nickel-clad copper ribbon leads. Options B-87 and B-129 both reduce fatigue life of WK Series gages, and should not be selected where best cyclic endurance is required. Internal tab connections are +770 F (+410 C) solder. Leadwires may be soft soldered, spot welded or silver soldered. Refer to M-M Bulletin B-132 for information on solders.

NOTE: The backing of WK Series gages has been specially treated for optimum bond formation with all appropriate strain gage adhesives. No further cleaning is necessary if contamination of the prepared surface is avoided during handling.

FORM 863618

WK-13-062AP-350
GAGE TYPE

350.0 ± 0.3%
RESISTANCE IN OHMS

2.23 ± 1.0%
GAGE FACTOR AT 75°F

−1.2%
K_t

DG-K14FF00
LOT NUMBER

5 GAGES
QUANTITY

TEMPERATURE-INDUCED APPARENT STRAIN   LOT NO. K14FF00

APPARENT MICROSTRAIN (Based on Instrument G.F. of 2.00)

GAGE FACTOR VARIATION (Typical)

24°C
APPARENT STRAIN
75°F
GAGE FACTOR

TEMPERATURE IN °CENTIGRADE

TEMPERATURE IN °FAHRENHEIT

TESTED ON: 2024-T4 ALUMINUM   CODE 863218   Q.A.

TEST PROCEDURES USED BY MICRO MEASUREMENTS
FOR STRAIN GAGE PERFORMANCE EVALUATION

QA MM JB

OPTICAL DEFECT ANALYSIS . . . . M-M Procedures and Standards
GAGE FACTOR AT 75 F . . . . ASTM E251-67 (Constant Stress Cantilever Method) *
G.F. VARIATION WITH TEMPERATURE . . . . ASTM E251-67 (Constant Stress Method)
APPARENT STRAIN VERSUS TEMPERATURE . . . . ASTM E251-67 (Slow Heating Rate, Continuously Recorded)
TRANSVERSE SENSITIVITY . . . . ASTM E251-67
INITIAL RESISTANCE . . . . M-M Procedure, Direct NBS Traceability on Resistance Standards
FATIGUE LIFE . . . . NAS 942 (Modified)
STRAIN LIMITS . . . . NAS 942 (Modified)
GAGE THICKNESS . . . . M-M Procedure

NOTE: This data is derived in an uniaxial stress field with Poisson's ratio of approximately .255

Fig. 19.   Specifications for the strain gages used to measure magneto-
striction.   Note that K alloy is a nickel chromium alloy.
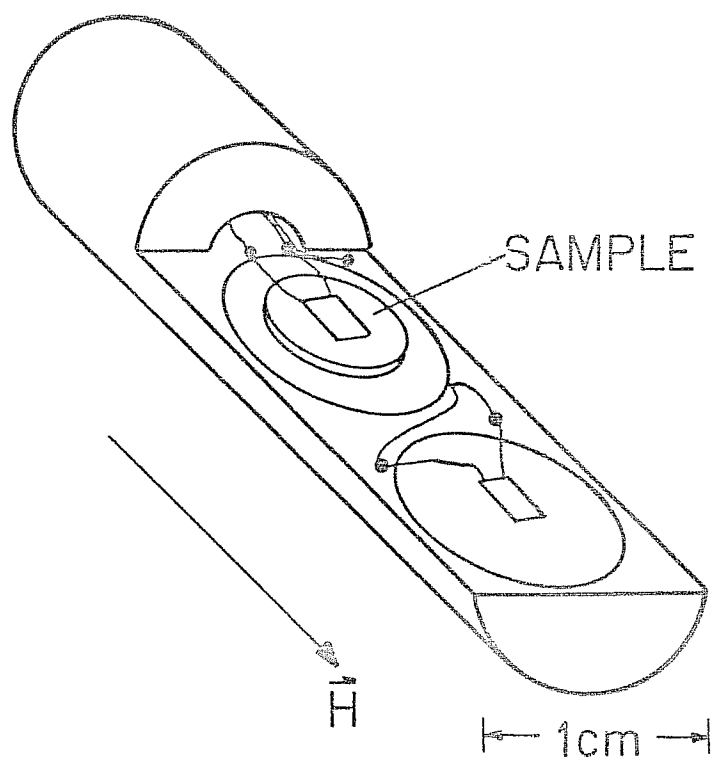
SAMPLE

$\vec{H}$

⊢— 1cm —⊣

Fig. 20. Mounted sample and dummy gages on brass dewar insert.

than 2 microstrain. An Au + 0.7 atomic % Fe vs. chromel thermo-couple measured the sample temperature. Thin-walled stainless steel tubing, soldered to the sample mount, was used to hold the sample in the dewar and to protect the thermocouple and lead wires.

The temperature of the sample was controlled by a Janis variable temperature dewar. The sample was cooled to either 77 or 4.2 K and strain vs. field curves were taken at a number of temperatures as the sample warmed slowly.

The two strain gages are connected as opposite arms of a Wheat-stone Bridge, as shown in Fig. 21. The magnetostrictive strain is proportional to the voltage output of the bridge.

$$(33) \quad V_{out}/V_{in} = F\epsilon/(4 + 2F\epsilon),$$

where F is the gage factor and ϵ is the strain. If $\epsilon < 3 \times 10^{-3}$, as was the case in this work, an error of less than 1 % is incurred by ignoring the factor of $2F\epsilon$ in eq. (33),[45] so that

$$(34) \quad V_{out}/V_{in} = \tfrac{1}{4}F\epsilon.$$

The magnetostriction was measured in fields up to 110 kOe. Since these fields are insufficient to saturate the sample except in the easy direction, it is important to understand how the measured strain is related to the magnetostriction. When a field is applied perpendicular to the c-axis, the angle between the magnetization and the c-axis is given by

$$(35) \quad \sin\theta = M_s H/2K_1$$

which follows from eq. (15) with $K_2 = 0$. For the measurement of λ_A,
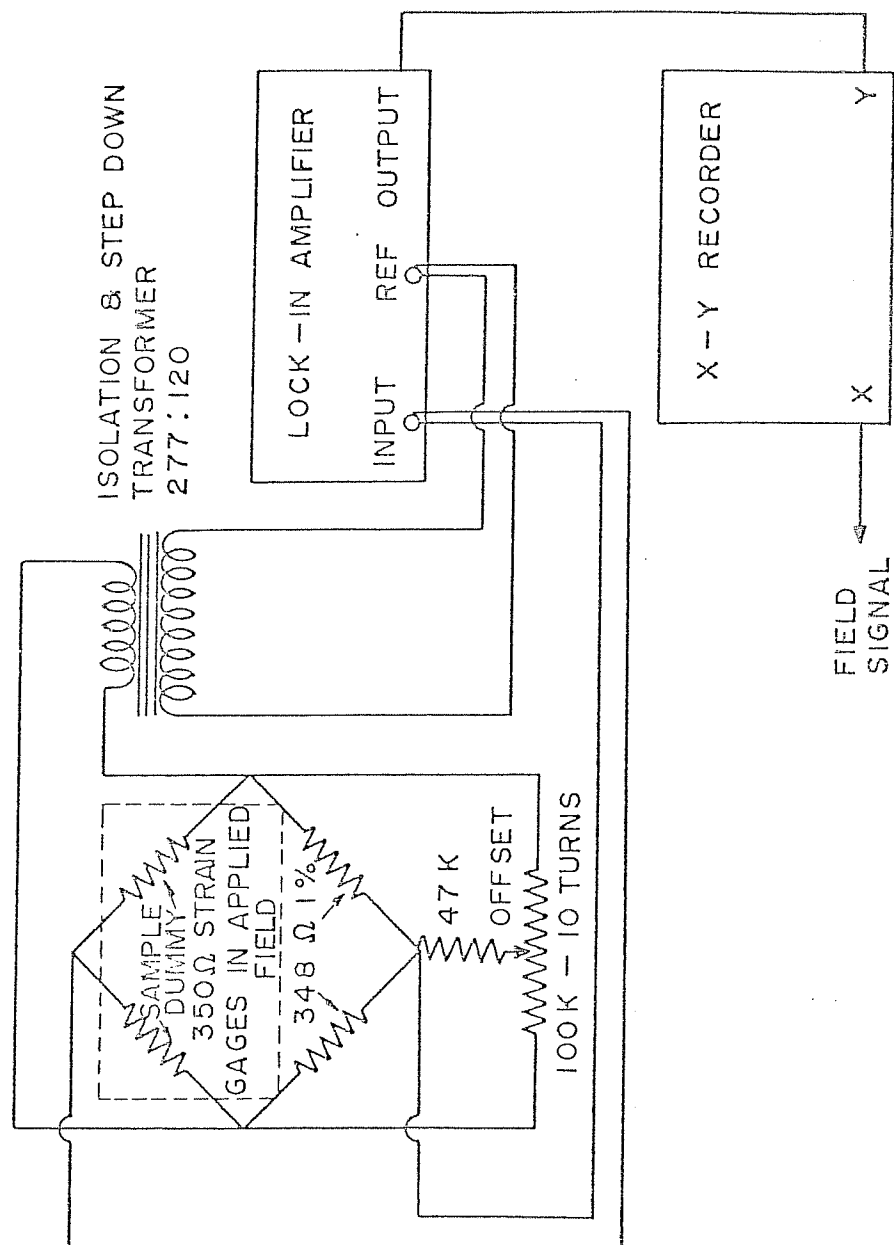
$$(36) \quad \epsilon = \lambda_A \sin^2\theta.$$

Fig. 21. Magnetostriction measuring circuit.

Substituting for sinθ from eq. (35) yields

$$(37) \quad \epsilon = \lambda_A (H M_s / 2 K_1)^2.$$

The strain is proportional to the field squared. In terms of the

input and output voltages of the Wheatstone Bridge, eq. (37) becomes

$$(38) \quad V_{out}/V_{in} = \lambda_A \tfrac{1}{4} F (H M_s / 2 K_1)^2.$$

Eq. (38) also applies to λ_B and λ_C since the magnetostriction is

proportional to $\sin^2\theta$ from Table IV. For the λ_D measurement, the

strain is linear in sinθ and the analogous equation is,

$$(39) \quad V_{out}/V_{in} = (4 \lambda_D - \lambda_A - \lambda_C) (F H M_s / 16 K_1) + \text{higher order}$$
$$\text{terms.}$$

A typical magnetostriction curve is shown in Fig. 22. Note that the

numerical values obtained for the magnetostriction coefficients

depend on the value of $(K_1)^2$; this is why it is so important to

measure magnetostriction and anisotropy on the same samples.

To determine the magnetostriction constants, it is necessary

to find the second order coefficient of the V_{out} vs. field curves

for λ_A, λ_B and λ_C, and the linear coefficient for λ_D. Since the

data are defined over a finite interval and the voltages can be read

at evenly spaced field values, the data can be fit to Chebychev

polynomials by a least squares method.[46] Fitting to a polynomial

avoids the two main faults of fitting to a power series: first, the

coefficients are calculated by solving the normal equations which are

unwieldy above second order and are ill-conditioned; and second, the

calculated coefficients depend on the chosen degree of the fitted

equation and do not converge as the degree is increased. In this

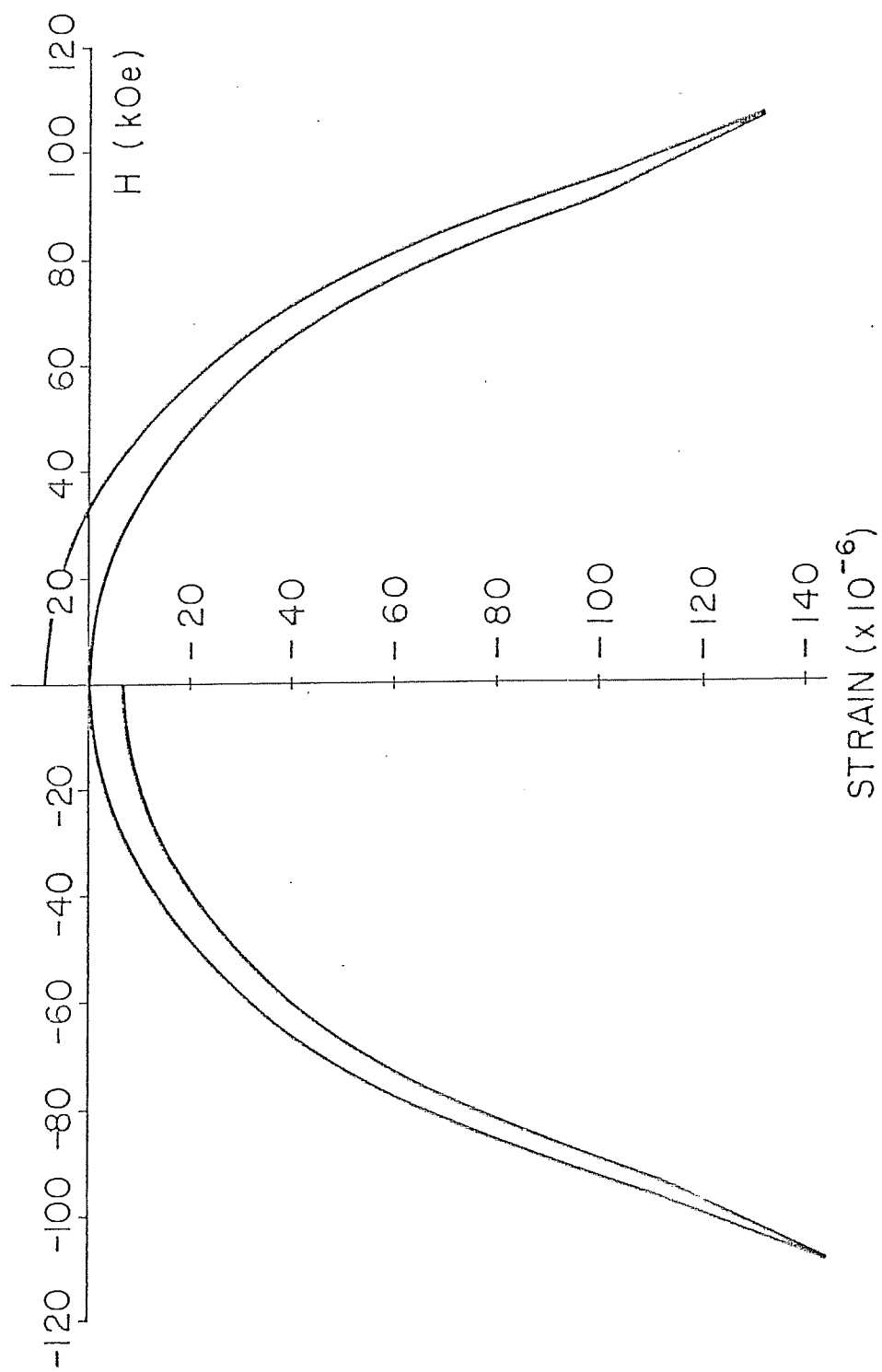case, the second objection is the most severe since it is the deter-

Fig. 22. Typical strain vs. field curve for λ_A. The voltage drift is due to the slow rise in sample temperature during the measurement; the mean temperature was 200 K.

mination of the first or second order coefficient that is most important rather than finding the best fit of a power series to the data. The program used to find the magnetostriction constants is listed in Program II.

One problem with this measurement is that several samples were shattered as the field was applied. In three cases, the sample broke into small pieces. It seems likely that these samples broke along preexisting cracks caused by spark cutting. In one case, a λ_C sample sheared itself in half by twisting in the field. This failure showed that the torque produced by the field exceeded the mechanical strength of the material. This problem usually occurred near 4.2 K where the anisotropy and saturation magnetization are highest, causing the largest torque on the sample. It is interesting to note that none of these failures was caused by failure of the epoxy. Each time, a complete layer of the sample remained attached to the sample holder.

Results

The magnetostriction constants are plotted in Figs. 23 and 24 as a function of temperature. The magnetostriction constants from eq. (26) are shown in Fig. 23 and the constants from eq. (27) are shown in Fig. 24.

This is the first time the magnetostriction of $SmCo_5$ has been reported below room temperature. The room temperature data of Doane[6] are also shown in Fig. 23. For a better comparison, her magnetostriction constants have been adjusted to the values for K_1 and M_s

```
1000 REM CHEBYCHEV POLYNOMIAL APPROXIMATION FOR EQUIDISTANT DATA
1010 DIM V(100),Y(100),E(100)
1020 DIM R(25),C(25),F(25),X(25),T(25)
1030 REM M=ORDER,N=# OF DATA PTS.,X(1)=LOWEST X,D=INCREMENT
1035 READ H,V
1040 READ N,X(1),D
1045 X(0)=X(1)-D
1050 FOR J=1 TO N
1055 READ Y(J)
1060 X(J)=X(J-1)+D
1065 NEXT J
1070 READ A$,B$
1075 PRINT A$,B$
1080 FOR M=2 TO 7
1100 REM COMPUTE ROOTS XBAR
1110 FOR I=0 TO M
1115 R(M+1-I)=COS(1.5708*(2*I+1)/(M+1))
1120 NEXT I
1200 REM NORMALIZE VECTORS
1205 V(1)=-1
1210 FOR I=1 TO N-1
1215 V(I+1)=V(I)+2/(N-1)
1220 NEXT I
1300 REM LAGRANGIAN INTERPOLATION
1310 I=1
1320 FOR L=1 TO N
1325 IF R(I)>V(L) THEN 1390
1330 U=(R(I)-V(L-1))/(V(L)-V(L-1))
1335 IF L>2 THEN 1350
1340 F(I)=U*(Y(L)-Y(L-1))+Y(L-1)
1345 GO TO 1360
1350 IF L)=N THEN 1340
1353 Z=-U*(U-1)*(U-2)*Y(L-2)/6+(U*U-1)*(U-2)*Y(L-1)/2
1356 F(I)=Z-(U+1)*(U-2)*U*Y(L)/2+U*(U*U-1)*Y(L+1)/6
1360 I=I+1
1370 IF (M+2)(=I THEN 1410
1375 IF R(I)(=V(L) THEN 1330
1390 NEXT L
1400 REM COMPUTE COEFFICIENTS
1410 FOR I=1 TO M+1
1415 S=0
1420 IF I=2 THEN 1445
1422 IF I)2 THEN 1470
1425 FOR J=1 TO M+1
1430 S=S+F(J)
1435 NEXT J
1440 GO TO 1520
1445 FOR J=1 TO M+1
1450 S=S+R(J)*F(J)
1455 NEXT J
1460 GO TO 1520
1470 V(1)=1
1480 FOR J=1 TO M+1
1485 V(2)=R(J)
1490 FOR K=3 TO I
1495 V(K)=2*R(J)*V(K-1)-V(K-2)
1500 NEXT K
1505 S=S+F(J)*V(I)
1510 NEXT J
1520 C(I)=2*S/(M+1)
1530 NEXT I
1540 C(1)=C(1)/2
```

```
1570 S1=(2*X(1)+(N-1)*D)/2
1575 S2=(N-1)*D/2
1580 PRINT "POLYNOMIAL COEFFICIENTS, DEGREE";M
1600 REM CONVERT CHEBYCHEV SERIES TO ITS EQUIVALENT POWER SERIES
1610 F(1)=C(1)\F(2)=C(2)
1620 IF M<=1 THEN 1810
1625 FOR K=1 TO M+1
1630 V(K)=0
1635 R(K)=0
1640 F(K+2)=0
1645 NEXT K
1650 V(2)=1
1660 FOR K=3 TO M+1
1665 R(1)=INT(COS(1.5708*(K-1))+.5)
1670 FOR J=2 TO K
1675 R(J)=2*V(J-1)-R(J)
1680 NEXT J
1690 FOR J=1 TO K
1695 F(J)=F(J)+C(K)*R(J)
1700 Z=V(J)
1705 V(J)=R(J)
1710 R(J)=Z
1715 NEXT J
1720 NEXT K
1800 REM GO BACK TO ORIGINAL INTERVAL
1810 R(1)=F(1)
1820 FOR K=2 TO M+1
1830 R(K)=0
1840 L=K-1
1850 R(K)=R(K)+F(K)/S2^L
1855 S3=1
1860 Z=1
1870 FOR J=1 TO L
1880 S3=S3*J
1890 Z=Z*(K-J)
1895 R(K-J)=R(K-J)+(Z*(-S1)^J*F(K))/(S3*S2^L)
1897 NEXT J
1900 NEXT K
2000 REM COMPUTE SAMPLE VARIANCE
2025 T=0
2030 REM Y(I) IS THE Y VALUE,V(I) IS THE CALCULATED VALUE
2040 FOR I=1 TO N
2050 V(I)=0
2060 FOR J=0 TO M
2065 V(I)=V(I)+R(J+1)*X(I)^J
2070 NEXT J
2075 T=T+(Y(I)-V(I))*(Y(I)-V(I))
2080 NEXT I
2085 REM T=SAMPLE VARIANCE
2090 T=T/(N-M-1)
2100 REM CALCULATE COEFFICIENT ERRORS
2105 REM Y1 IS COEFFICIENT NECESSARY FOR PERFECT FIT
2107 REM T(J) IS MAXIMUM R. M. S. ERROR FOR COEFFICIENT
2110 FOR J=0 TO M
2115 T1=0
2120 FOR I=1 TO N
2122 IF X(I)=0GO TO 2160
2125 Y=0
2130 Y=V(I)-R(J+1)*X(I)^J
2150 Y1=(Y(I)-Y)/X(I)^J
2155 T1=T1+(Y1-R(J+1))^2
2160 NEXT I
2165 T(J+1)=SQR(T1)/(N-M-1)
2170 NEXT J
2200 REM PRINTOUT
2210 FOR K=0 TO M
```

```
2215 Z=V/H^K
2220 PRINT K,R(K+1)*Z,T(K+1)*Z
2230 NEXT K
2240 PRINT "SAMPLE VARIANCE =";T
2300 NEXT M
2400 FOR I=1 TO N
2410 PRINT Y(I);
2420 NEXT I
2450 READ V
2455 T=273.768+46.4274*V-.76637*V*V
2460 PRINT "TEMPERATURE =";INT(T+.5);"K"
2465 G=2.34726-3.08105E-04*T-2.96489E-07*T*T
2470 PRINT "GAGE FACTOR =";INT(G*100+.5)/100
2500 DATA 12450,4.00000E-06
2510 DATA 17,-4,.5
2520 DATA 2.4,1.3,.6,.3,.4,.4,.4,.6
2530 DATA .5,.4,.9,.9,1.2,1.8,2.45,3.1,3.7
2540 DATA "MAY 17, 1978"
2550 DATA "#7"
2560 DATA -3.964
9999 END
```
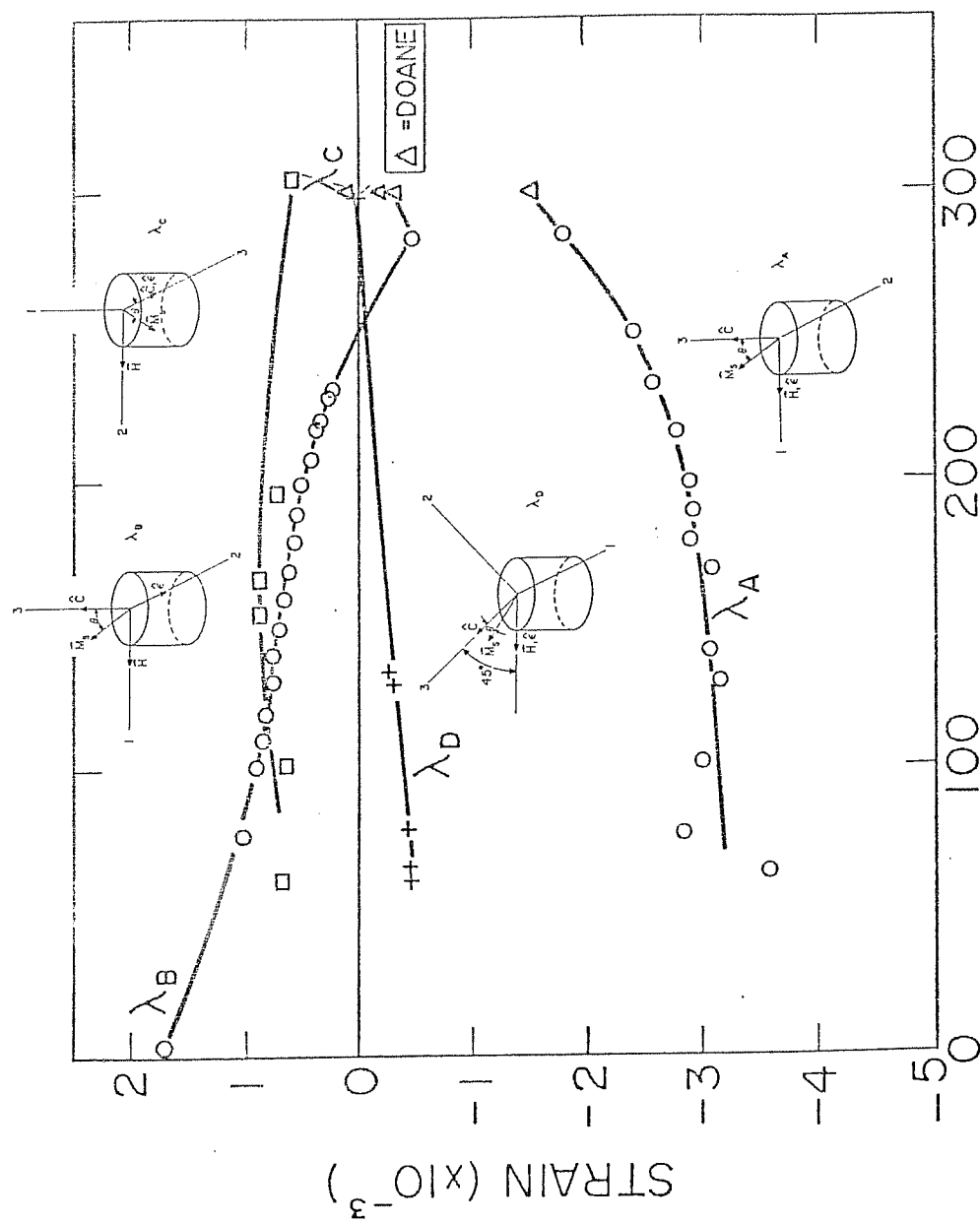
Fig. 23. Magnetostriction vs. temperature, constants from eq. (26) and reference 42. Also shown are the data of Doane6 at 300 K and the measurement orientations used for each constant.
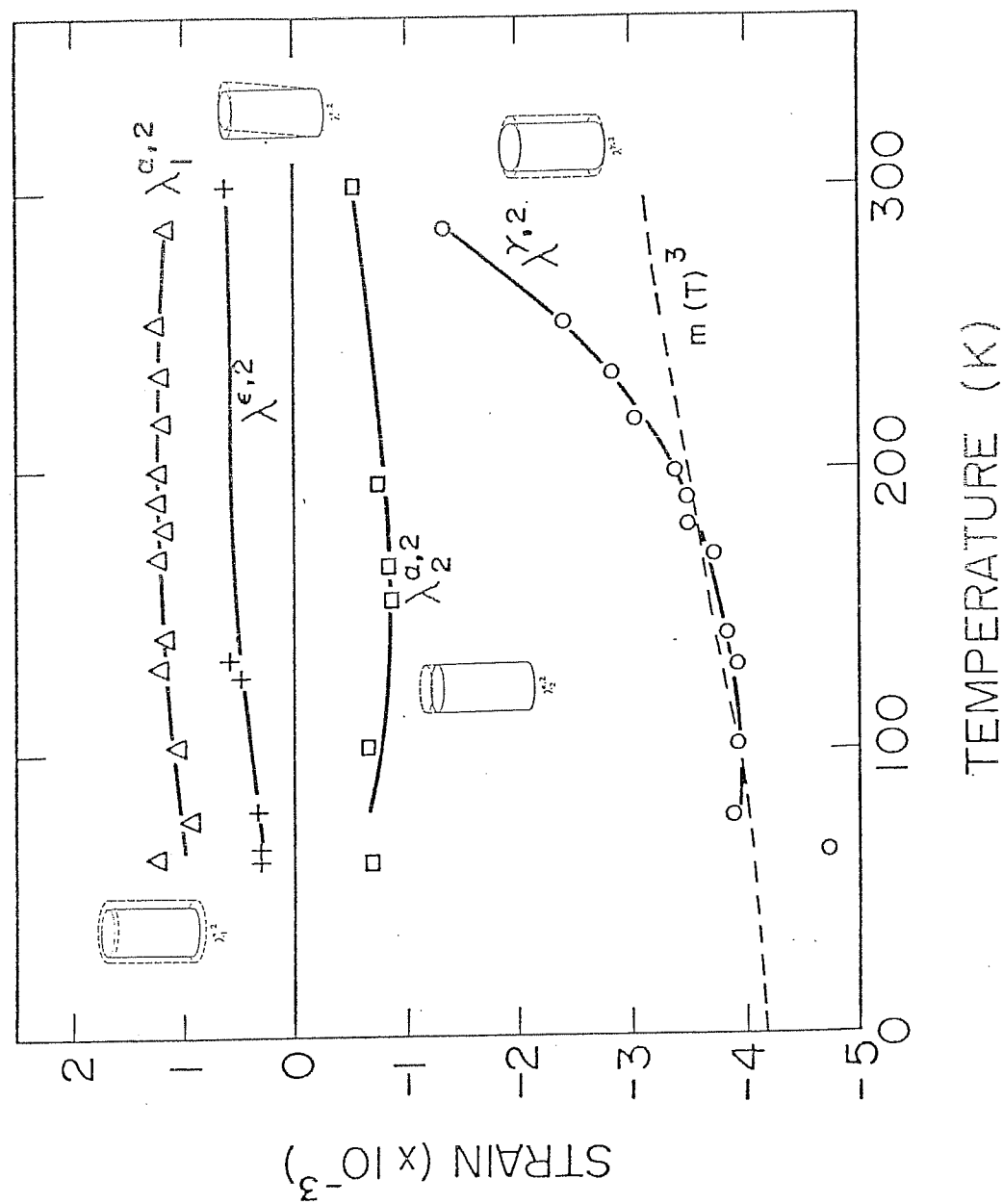
Fig. 24. Magnetostriction vs. temperature, constants from eq. (27) and reference 32. Also shown is the deformation corresponding to each constant.

found in this work. The adjustment increases her values by a factor of two. There is fair agreement between the room temperature values and Doane's results, although λ_D in this experiment is nearly zero at room temperature. The only magnetostriction constant to change sign is λ_B; the crossover occurs near 250 K.

As mentioned earlier, the Callen and Callen theory[24] may apply on a limited scale to the temperature dependence on the magneto-striction of $SmCo_5$. To make the comparison, the data in Fig. 24 should be compared to eq. (29). This comparison shows that $\lambda^{\gamma,2}$ has a much stronger temperature dependence than $m(T)^3$ and the other three magnetostriction constants are almost temperature independent. From this comparison it is clear that the temperature dependence of the magnetostriction of $SmCo_5$ cannot be predicted by the Callen and Callen theory.

The dominant error in the measurement is the uncertainty of K_1. Eq. (38) shows that all the magnetostriction constants except λ_D and $\lambda^{\epsilon,2}$ depend on K_1^2; λ_D depends on K_1, λ_A and λ_C. The estimated uncertainty of this measurement varies from about 25% at room temperature up to about 60% at 4.2 K.

CHAPTER VI

SUMMARY AND DISCUSSION

To obtain a complete set of data on the intrinsic magnetic properties of $SmCo_5$, the saturation magnetization, magneto-crystalline anisotropy and magnetostriction of single crystal samples have been measured as a function of temperature from 4.2 K to room temperature and above. Because of the large anisotropy of this compound, it is not possible to rotate the moment completely into the hard direction of magnetization even in the maximum available field of 110 kOe. In this case it is necessary to know the saturation magnetization in order to determine the anisotropy, and to know both the saturation magnetization and the anisotropy in order to determine the magnetostriction. Making all the measurements on one set of single crystal samples cut from the same ingot thus increases the accuracy of the results.

The saturation magnetization was measured up to 883 K, using a vibrating sample magnetometer. The data are in good agreement with previous results and values calculated for 0 K. At 295 K, σ_s = 98.8 emu/g corresponding to M_s = 845 emu/cm^3 with a measured density of 8.559 g/cm^3. Below 220 K, the data are consistant with the $T^{3/2}$ temperature dependence predicted by Bloch.[27] Comparison of the data to the Brillouin function with J = ½ and J = 1 shows that the samarium sublattice may have a small moment at low temperatures and a stronger temperature dependence than the cobalt sublattice.

72

Magnetocrystalline anisotropy was measured by the torque method in a maximum field of 65.6 kOe from 4.2 to 410 K. At 302 K, $K_1 = 2.4 \times 10^8$ erg/cm^3 and at 4.2 K, $K_1 = 3.2 \times 10^8$ erg/cm^3. K_1 decreases monotonically with increasing temperature; K_2 is negligible at all measuring temperatures. The measured values of K_1 from SmCo$_5$ are larger than most previous results by up to 30%. However, considering the uncertainty of this and other measurements, the results probably agree within the experimental error. There is good agreement between the measured temperature dependence and the Callen and Callen theory[24] below 300 K.

Magnetostriction constants have been measured using strain gages at maximum fields of 110 kOe and at temperatures from 4.2 to 300 K; this is the first such measurement below room temperature. The measured strains at room temperature are in agreement with those of Doane.[6] Using the notation of Mason,[42] the room temperature values of the magnetostriction are $\lambda_A = -1800$, $\lambda_B = -470$, $\lambda_C = +580$ and $\lambda_D = +45$, all in units of 10^{-6}. The uncertainty of the measured anisotropy affects the uncertainty of the magnetostriction constants since they depend on $K_1{}^2$. However, the relative temperature dependence of each constant is measured to within 10%.

Origin of the Coercive Field in SmCo$_5$ Permanent Magnets

The coercive field of a permanent magnet is not an intrinsic property of the material such as the saturation magnetization, anisotropy, magnetostriction or Curie temperature. The forces that determine the coercive field are complicated and often difficult to control.

Since the coercive field is of extreme practical importance, it is desirable to see if any intrinsic magnetic properties influence the coercive field.

The largest possible coercive field in a material such as $SmCo_5$, where the anisotropy is dominated by the magnetocrystalline anisotropy, is $H_{ci}(max) = 2 K_1/M_s$. This corresponds to the coherent rotation of the magnetization in single domain particles. As the name indicates, single domain particles do not break up into domains in zero field; however, they are limited in size by a critical balance between the anisotropy and the magnetostatic energies,

$$(40) \quad L_c = \frac{1.7 \gamma}{(\pi M_s)^2},$$

where γ is the domain wall energy. The critical size for a single domain particle of $SmCo_5$ is about $1 \mu m$.[47] At 300 K, $2 K_1/M_s = 568$ kOe while the best coercive fields in commercial $SmCo_5$ permanent magnets range from 20 to 30 kOe. Yet these coercive fields are obtained from powders with an average particle size of 10 to 20 μm.[9] Clearly coherent rotation is not the coercivity mechanism; the magnetization must reverse by domain wall motion.

Magnetization reversal by domain wall motion can be governed by domain wall pinning or domain wall nucleation. If domain walls are easily nucleated in a reverse field, the coercivity is controlled by the difficulty of domain wall motion through the material, due to second phase precipitates or other disturbances in the lattice. In such a case, the coercivity is controlled by domain wall pinning. In contrast, if a large reverse field is required to nucleate a domain

wall but once created, it moves freely through the material, the coercivity is governed by domain wall nucleation.

It is possible to determine which coercivity mechanism is operating by examining the behavior of a thermally demagnetized sample when it is first magnetized. Fig. 25 shows magnetization curves for both cases. The upper curve shows a wall nucleation material and the lower curve shows a wall pinning material. Domain walls already exist in a thermally demagnetized material since they are easily nucleated just below the Curie temperature. In the wall nucleation material shown in the upper curve of Fig. 25, the domain walls move freely when the first field is applied. Therefore, a field much smaller than the coercive field can saturate a thermally demagnetized wall nucleation material. In the wall pinning material shown in the lower curve of Fig. 25, the domain walls are not helpful in reversing the magnetization. A field nearly equal to the coercive field is required to unpin the domain walls to saturate the material.

The coercive field of $SmCo_5$ permanent magnets is based on wall nucleation since the magnetization curves of thermally demagnetized samples resemble the upper curve in Fig. 25.[9] This explains why $SmCo_5$ permanent magnets are prepared from powders. In a powder, the nucleation of a single domain wall will reverse the magnetization in a single small particle. Nucleation must occur in roughly half the particles in the powder for the magnetization to be reduced to zero. It is thought that the domain walls in sintered $SmCo_5$ permanent magnets nucleate in areas of locally lower anisotropy or at irregular particle
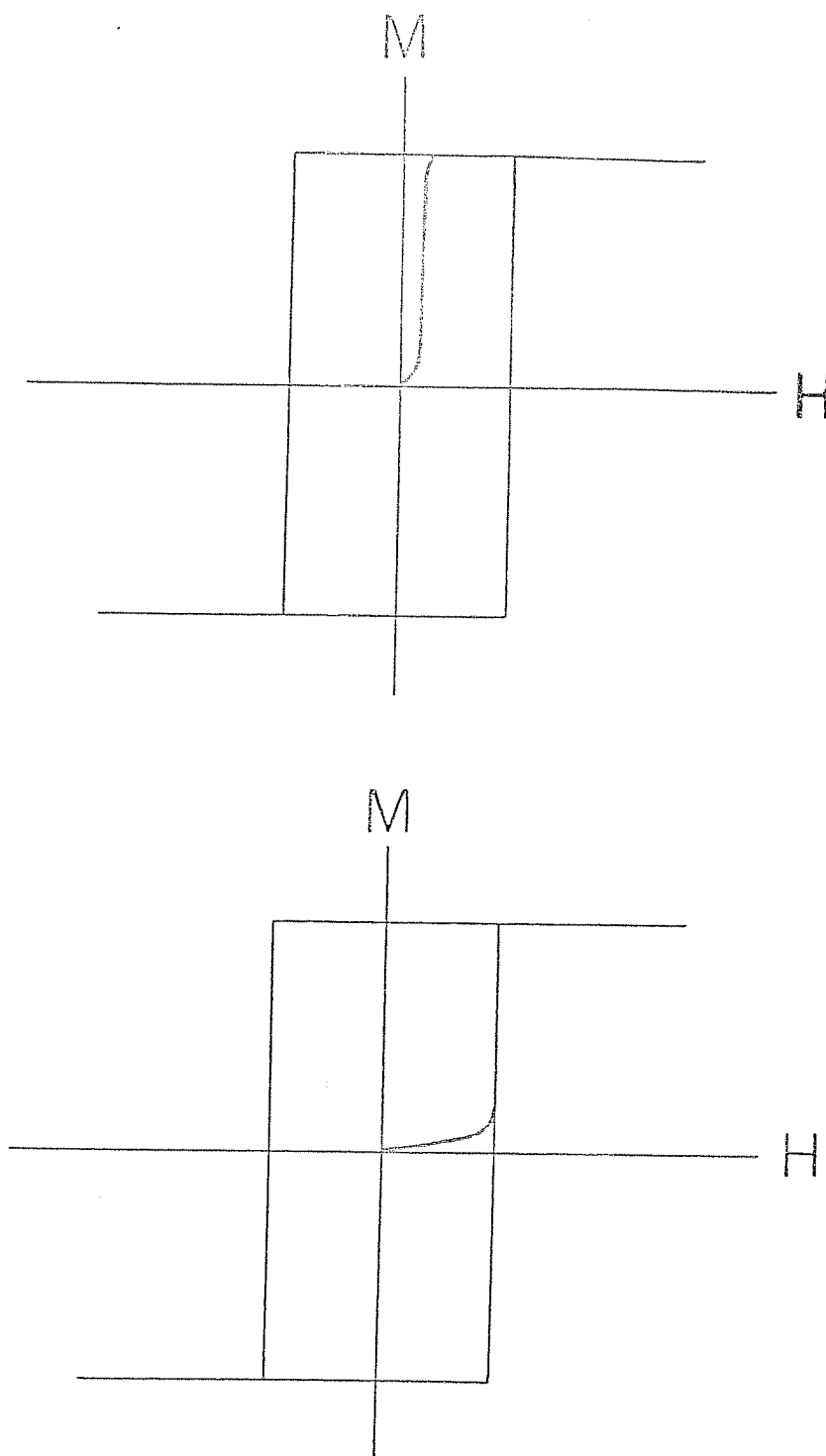
Fig. 25. Magnetization curves of thermally demagnetized samples
showing a domain nucleation material (upper curve) and
a domain pinning material (lower curve).

edges.[47] Local deviations in the anisotropy could be from local compositional variations caused by preferential oxidation of the samarium. Irregular particle edges cause high demagnetizing fields which favor domain wall nucleation.

One factor that makes domain wall nucleation difficult in $SmCo_5$ permanent magnets is the large magnetostriction. Since $SmCo_5$ is uniaxial, eq. (26) shows that there is no magnetostriction when the magnetization is parallel to the c-axis. In a domain wall, the rotation of the local moments away from the c-axis would give rise to magnetostrictive strains if the domain wall were free to deform. However, the domain wall is constrained by the surrounding crystal and no magnetostrictive strains can occur. The crystal itself does work on the domain wall against the magnetostriction to confine the wall. This work against magnetostriction is part of the domain wall energy. The energy to nucleate a domain wall must be supplied by the reverse field. Therefore, the larger the magnetostriction, the larger the field required to nucleate a domain wall and the larger the coercivity in a material where the coercivity is governed by domain wall nucleation.

Doane has proposed a model for the coercive field in sintered $SmCo_5$ permanent magnets that considers the effect of magnetostriction on the energy of the domain wall. She shows that the magnetostatic contribution to the domain wall energy of $SmCo_5$ is dominated by λ_A because it has the largest absolute value and hence the greatest effect on the coercivity. The model further predicts that the temperature dependence of the coercive field should vary as the temperature depen-

dence of λ_A/M_S. This quantity is plotted in Fig. 26, normalized to unity at 64 K, since it is the lowest temperature where λ_A was measured. The error bars on λ_A/M_S represent an uncertainty of 12% which is the estimated error of the temperature dependence of λ_A/M_S. Also plotted are the normalized intrinsic coercive fields of three high-quality $SmCo_5$ permanent magnets.[41] There seems to be some agreement between the model and the experimental results. Since this model only considers the magnetostrictive contribution to the domain wall energy, Doane expected the model to have a stronger temperature dependence than the coercive field. The normalized K_1 vs. temperature results are also plotted in Fig. 26 to show that the temperature dependence of the coercive field is much stronger than the temperature dependence of the anisotropy.

The temperature dependence of the coercive field of $SmCo_5$ permanent magnets was also considered by Kütterer et al.[48] Their work shows that the temperature dependence of the coercive field depends on the absolute value of the coercive field. For high coercivity magnets, they claim that the coercivity may be controlled by pinning of domain walls by atomic disorder. They derive the temperature dependence as

$$(41) \quad H_c(T) \sim M_S^2 \ (K_1/M_S)^{5/4}.$$

The shape of this curve is not too different from λ_A/M_S. They also find that the coercivity mat follow a K_1/M_S temperature dependence, if the anisotropy of Sm_2Co_{17} is used, since the low coercivity regions in $SmCo_5$ permanent magnets may have anisotropies closer to Sm_2Co_{17} than to $SmCo_5$.
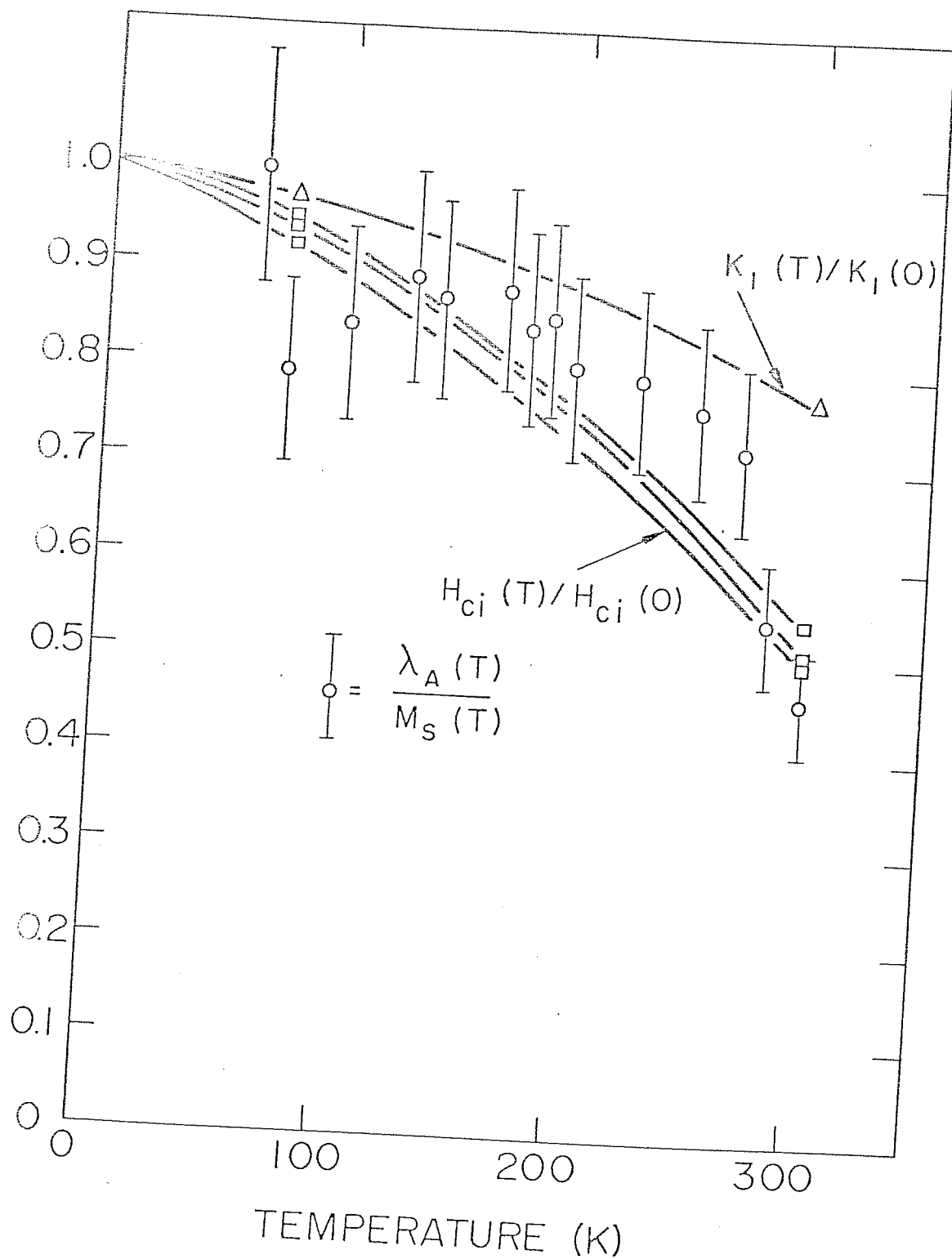
Fig. 26. Normalized (λ_A/M_s), K_1 and H_{ci} vs. temperature. The quantity (λ_A/M_s) is normalized to unity at 64 K, the lowest temperature at which λ_A was measured. The H_{ci} data if from reference 41.

REFERENCES

1.   G. W. Urbain, P. Weiss and F. Trombe, Comptes Rendus 200 (1935) 2132.

2.   Jack E. Powell, Chapter 5 in The Rare Earths, F. H. Spedding and A. H. Daane eds. Krieger Publishing Co. Inc., Huntington, N. Y. (1971).

3.   K. Nassau, L. V. Cherry and W. E. Wallace, J. Phys. Chem. Solids 16 (1960) 123.

4.   W. M. Hubbard, E. Adams and J. V. Gilfrich, J. Appl. Phys. 31 (1960) 3683.

5.   G. Hoffer and K. J. Strnat, IEEE Trans. Magnetics 2 (1966) 487.

6.   D. A. Doane, Ph.D. Thesis, University of Pennsylvania (1976).
     D. A. Doane and C. D. Graham, Jr., AIP Conf. Proc. 18 (1974) 1192.
     D. A. Doane, J. Appl. Phys. 48 (1977) 2062.

7.   J. J. Becker, J. Appl. Phys. 41 (1970) 1055.

8.   D. L. Martin and M. G. Benz, AIP Conf. Proc. 5 (1972) 970.

9.   A. Menth, H. Nagel and R. S. Perkins in Annual Review of Materials Science, Huggins, Bube and Roberts eds., Annual Reviews Inc., Palo Alto, Calif. Vol. 8 (1978).

10. E. Tatsumoto, T. Okamoto, H. Fujii and C. Inoue, Suppl. J. de Physique 32 (1971) C1-550.

11. M. G. Benz and D. L. Martin, Appl. Phys. Lett. 17 (1970) 176.

12. Y. Tawara and K. Strnat, IEEE Trans. Magnetics 12 (1976) 954.

13. R. L. Bergner, H. A. Leupold, J. R. Shapirio, A. Tauber and F. Rothwarf, to be published in J. Appl. Phys.

14. H. Nagel, AIP Conf. Proc. 29 (1976) 603.

15. R. W. Lee, to be published in J. Appl. Phys.

16. D. V. Ratnam and M. G. H. Wells, AIP Conf. Proc. 18 (1974) 1154.

17. D. K. Das, AIP Conf. Proc. 10 (1973) 628.

18. A. Menth, AIP Conf. Proc. 29 (1976) 600.

19. R. L. Bergner, H. A. Leupold, J. T. Breslin, F. Rothwarf and A. Tauber, to be published in J. Appl. Phys.

20. A. E. Austin and J. F. Miller, Battelle Columbus Laboratories Interim Report IV to Wright-Paterson Air Force Base (1972).

21. K. H. J. Buschow and W. A. J. J. Velge, Z. angew. Physik 26 (1969) 157.

22. S. E. Haszko, Trans. Met. Soc. AIME 218 (1960) 763.

23. C. W. Searle, W. G. D. Frederick and H. J. Garrett, IEEE Trans. Magnetics 9 (1973) 164.

24. Earl Callen and Herbert B. Callen, Phys. Rev. 139 (1965) A455 and 129 (1963) 578.

25. D. L. Martin, M. G. Benz and A. C. Rockwood, AIP Conf. Proc. 10 (1973) 583.

26. P. Weiss, J. de Physique 6 (1907) 661.

27. F. Bloch, Z. Physik 61 (1930) 206.

28. S. Chikazumi, Physics of Magnetism, Wiley, New York (1964).

29. H. P. Klein and A. Menth, AIP Conf. Proc. 18 (1974) 1177.
    H. P. Klein, A. Menth and R. S. Perkins, Physica 80B (1975) 153.

30. A. S. Ermolenko, Proc. Int. Conf. on Magn. 1(1) (1974) 231.

31. E. A. Nesbitt and J. H. Wernick, Rare Earth Permanent Magnets, Academic Press, New York (1973).

32. A. E. Clark, B. F. DeSavage and R. Bozorth, Phys. Rev. 138 (1965) A216.

33. C. Zener, Phys. Rev. 96 (1954) 1355.

34. H. B. Callen and E. Callen, J. Phys. Chem Solids 27 (1966) 1271.

35. M. I. Darby and E. D. Isaac, IEEE Trans. Magnetics 10 (1974) 259.

36. J. E. Greedan and V. U. S. Rao, J. Sol. State Chem. 6 (1973) 387.

37. B. D. Cullity, Introduction to Magnetic Materials, Addison-Wesley, Reading, Mass. (1972).

38. W. Sucksmith and J. E. Thompson, Proc. Roy. Soc. A255 (1954) 362.

39. S. G. Sankar, V. U. S. Rao, E. Segal, W. E. Wallace, W. G. D. Frederick and H. J. Garrett, Phys. Rev. 11B (1975) 435.

40. B. Barbara and M. Uehara, IEEE Trans. Magnetics 12 (1976) 997.

41. S. R. Trout, M. S. Thesis, University of Pennsylvania (1976).

42. W. P. Mason, Phys. Rev. 96 (1954) 302.

43. J. E. Goldman, Phys. Rev. 72 (1947) 529.
     J. E. Goldman and R. Smoluchowski, Phys. Rev. 75 (1949) 140.

44. R. Gersdorf, Ph.D. Thesis, University of Amsterdam (1961).

45. Micro Measurements, Tech Note TN-139-2 (1976).

46. Shan S. Kuo, Computer Applications of Numerical Methods, Addison-Wesley, Reading, Mass. (1972).

47. J. D. Livingston, AIP Conf. Proc. 10 (1973) 643.

48. R. Kutterer, H. R. Hilzinger and H. Kronmuller, J. Mag. Magn. Mat. 4 (1977) 1.

49. R. L. Streever, Phys. Letters 65A (1978) 360.

50. K. Niira, Phys. Rev. 117 (1960) 129.

BIBLIOGRAPHY

AUSTIN, A. E. and J. F. Miller, Battelle Columbus Laboratories Interim Report IV to Wright-Patterson Air Force Base (1972).

BARBARA, B. and M. Uehara, IEEE Trans. Magnetics $\underline{12}$ (1976) 997.

BECKER, J. J., J. Appl. Phys. $\underline{41}$ (1970) 1055.

BENZ, M. G. and D. L. Martin, Appl. Phys. Lett. $\underline{17}$ (1970) 176.

BERGNER, R. L., H. A. Leupold, J. T. Breslin, F. Rothwarf and A. Tauber, to be published in J. Appl. Phys.

BERGNER, R. L., H. A. Leupold, J. R. Shapirio, A. Tauber and F. Rothwarf, to be published in J. Appl. Phys.

BLOCH, F., Z. Physik $\underline{61}$ (1930) 206.

BUSCHOW, K. H. J. and W. A. J. J. Velge, Z. angew. Physik $\underline{26}$ (1969) 157.

CALLEN, Earl and Herbert B. Callen, Phys. Rev. $\underline{139}$ (1965) A455.

CALLEN, Earl and Herbert B. Callen, Phys. Rev. $\underline{129}$ (1963) 578.

CALLEN, H. B. and E. Callen, J. Phys. Chem. Solids $\underline{27}$ (1966) 1271.

CHIKAZUMI, S., Physics of Magnetism, Wiley, New York (1964).

CLARK, A. E., B. F. DeSavage and R. Bozorth, Phys. Rev. $\underline{138}$ (1965) A216.

CULLITY, B. D., Introduction to Magnetic Materials, Addison-Wesley, Reading, Mass. (1972).

DARBY, M. I. and E. D. Isaac, IEEE Trans. Magnetics $\underline{10}$ (1974) 259.

DAS, D. K., AIP Conf. Proc. $\underline{10}$ (1973) 628.

DOANE, D. A., Ph.D. Thesis, University of Pennsylvania (1976).

DOANE, D. A. and C. D. Graham, Jr., AIP Conf. Proc. $\underline{18}$ (1974) 1192.

DOANE, D. A., J. Appl. Phys. $\underline{48}$ (1977) 2062.

ERMOLENKO, A. S., Proc. Int. Conf. on Magn. $\underline{1(1)}$ (1974) 231.

GERSDORF, R., Ph.D. Thesis, University of Amsterdam (1961).

GOLDMAN, J. E., Phys. Rev. 72 (1947) 529.

GOLDMAN, J. E. and R. Smoluchowski, Phys. Rev. 75 (1949) 140.

GREEDAN, J. E. and V. U. S. Rao, J. Sol. State Chem. 6 (1973) 387.

HASZKO, S. E., Trans. Met. Soc. AIME 218 (1960) 763.

HOFFER, G. and K. J. Strnat, IEEE Trans. Magnetics 2 (1966) 487.

HUBBARD, W. M., E. Adams and J. V. Gilfrich, J. Appl. Phys. 31 (1960) 3683.

KLEIN, H. P. and A. Menth, AIP Conf. Proc. 18 (1974) 1177.

KLEIN, H. P., A. Menth and R. S. Perkins, Physica 80B (1975) 153.

KUO, Shan S., Computer Applications of Numerical Methods, Addison-Wesley, Reading, Mass. (1972).

KÜTTERER, R., H. R. Hilzinger and H. Kronmüller, J. Mag. Magn. Mat. 4 (1977) 1.

LEE, R. W., to be published in J. Appl. Phys.

LIVINGSTON, J. D., AIP Conf. Proc. 10 (1973) 643.

MARTIN, D. L. and M. G. Benz, AIP Conf. Proc. 5 (1972) 970.

MARTIN, D. L., M. G. Benz and A. C. Rockwood, AIP Conf. Proc. 10 (1973) 583.

MASON, W. P., Phys. Rev. 96 (1954) 302.

MENTH, A., H. Nagel and R. S. Perkins in Annual Review of Materials Science, Huggins, Bube and Roberts eds., Annual Reviews Inc., Palo Alto, Calif. Vol. 8 (1978).

MENTH, A., AIP Conf. Proc. 29 (1976) 600.

MICRO MEASUREMENTS, Tech Note TN-139-2 (1976).

NAGEL, H., AIP Conf. Proc. 29 (1976) 603.

NASSAU, K., L. V. Cherry and W. E. Wallace, J. Phys. Chem. Solids 16 (1960) 123.

NESBITT, E. A., and J. H. Wernick, Rare Earth Permanent Magnets, Academic Press, New York (1973).

NIIRA, K., Phys. Rev. 117 (1960) 129.

POWELL, Jack E., Chapter 5 in The Rare Earths, F. H. Spedding and A. H. Daane eds. Krieger Publishing Co., Inc., Huntington, N. Y. (1971).

RATNAM, D. V. and M. G. H. Wells, AIP Conf. Proc. 18 (1974) 1154.

SANKAR, S. G., V. U. S. Rao, E. Segal, W. E. Wallace, W. G. D. Frederick and H. J. Garrett, Phys. Rev. 11B (1975) 435.

SEARLE, C. W., W. G. D. Frederick and H. J. Garrett, IEEE Trans. Magnetics 9 (1973) 164.

STREEVER, R. L., Phys. Letters 65A (1978) 360.

SUCKSMITH, W. and J. E. Thompson, Proc. Roy. Soc. A225 (1954) 362.

TATSUMOTO, E., T. Okamoto, H. Fujii and C. Inoue, Suppl. J. de Physique 32 (1971) C1-550.

TAWARA, Y., and K. Strnat, IEEE Trans. Magnetics 12 (1976) 954.

TROUT, S. R., M. S. Thesis, University of Pennsylvania (1976).

URBAIN, G. W., P. Weiss and F. Trombe, Comtes Rendus 200 (1935) 2132.

WEISS, P., J. de Physique 6 (1907) 661.

ZENER, C., Phys. Rev. 96 (1954) 1355.